



HAL
open science

Evaluation of the Oh, Dubois and IEM backscatter models using a large dataset of SAR data and experimental soil measurements

M. Choker, N Baghdadi, Mehrez Zribi, Mohammad El Hajj, S. Paloscia, N.E.C. Verhoest, H. Lievens, F. Mattia

► To cite this version:

M. Choker, N Baghdadi, Mehrez Zribi, Mohammad El Hajj, S. Paloscia, et al.. Evaluation of the Oh, Dubois and IEM backscatter models using a large dataset of SAR data and experimental soil measurements. *Water*, 2017, 9 (38), 27 p. 10.3390/w9010038 . hal-01555470

HAL Id: hal-01555470

<https://hal.science/hal-01555470>

Submitted on 5 Sep 2017

HAL is a multi-disciplinary open access archive for the deposit and dissemination of scientific research documents, whether they are published or not. The documents may come from teaching and research institutions in France or abroad, or from public or private research centers.

L'archive ouverte pluridisciplinaire **HAL**, est destinée au dépôt et à la diffusion de documents scientifiques de niveau recherche, publiés ou non, émanant des établissements d'enseignement et de recherche français ou étrangers, des laboratoires publics ou privés.

Choker M., Baghdadi N., Zribi M., El Hajj M., Paloscia S., Verhoest N., Lievens H., Mattia F., 2017. Evaluation of the Oh, Dubois and IEM models using large dataset of SAR signal and experimental soil measurements. *Water*, 9(38), pp. 1-27, doi: 0.3390/w9010038.

1 Article

2 Evaluation of the Oh, Dubois and IEM backscatter 3 models using a large dataset of SAR data and 4 experimental soil measurements

5 Mohammad Choker¹, Nicolas Baghdadi¹, Mehrez Zribi², Mohammad El Hajj¹, Simonetta
6 Paloscia³, Niko E.C. Verhoest⁴, Hans Lievens^{4,5}, Francesco Mattia⁶

7 ¹ IRSTEA, UMR TETIS, 500 rue François Breton, F-34093 Montpellier cedex 5, France ;
8 E-Mails : mohammad.choker@teledetection.fr; nicolas.baghdadi@teledetection.fr; mohammad.el-
9 hajj@teledetection.fr

10 ² CESBIO, 18 av. Edouard Belin, bpi 2801, 31401Toulouse cedex 9, France;
11 E-Mails: mehrez.zribi@ird.fr

12 ³ CNR-IFAC, via Madonna del Piano 10, 50019 Sesto Fiorentino, Firenze, Italy;
13 E-Mail: s.paloscia@ifac.cnr.it

14 ⁴ Laboratory of Hydrology and Water Management, Ghent University, Ghent B-9000, Belgium;
15 E-Mails: niko.verhoest@UGent.be ; hans.lievens@UGent.be

16 ⁵ Global Modeling and Assimilation Office, NASA Goddard Space Flight Center, Greenbelt, MD 20771
17 USA.

18 ⁶ CNR-ISSIA, via Amendola 122/D, Bari 70126, Italy; E-Mail: mattia@ba.issia.cnr.it

19 Academic Editor: name

20 Received: date; Accepted: date; Published: date

21 **Abstract:** The aim of this paper is to evaluate the most used radar backscattering models (Integral
22 Equation Model "IEM", Oh, Dubois, and Advanced Integral Equation Model "AIEM") using a wide
23 dataset of SAR (Synthetic Aperture Radar) data and experimental soil measurements. These
24 forward models reproduce the radar backscattering coefficients (σ°) from soil surface
25 characteristics (dielectric constant, roughness) and SAR sensor parameters (radar wavelength,
26 incidence angle, polarization). The analysis dataset is composed of AIRSAR, SIR-C, JERS-1,
27 PALSAR-1, ESAR, ERS, RADARSAT, ASAR and TerraSAR-X data and in situ measurements (soil
28 moisture and surface roughness). Results show that Oh model version developed in 1992 gives the
29 best fitting of the backscattering coefficients in HH and VV polarizations with RMSE values of 2.6
30 dB and 2.4 dB, respectively. Simulations performed with the Dubois model show a poor
31 correlation between real data and model simulations in HH polarization (RMSE = 4.0 dB) and
32 better correlation with real data in VV polarization (RMSE = 2.9 dB). The IEM and the AIEM
33 simulate the backscattering coefficient with high RMSE when using a Gaussian correlation
34 function. However, better simulations are performed with IEM and AIEM by using an exponential
35 correlation function (slightly better fitting with AIEM than IEM). Good agreement was found
36 between the radar data and the simulations using the calibrated version of the IEM modified by
37 Baghdadi (IEM_B) with bias less than 1.0 dB and RMSE less than 2.0 dB. These results confirm
38 that, up to date, the IEM modified by Baghdadi (IEM_B) is the most adequate to estimate soil
39 moisture and roughness from SAR data.

40 **Keywords:** Oh; Dubois; IEM; AIEM; SAR images; soil moisture; and surface roughness.

42 1. Introduction

43 In the context of sustainable development, soil and water resources management is a key issue
44 not only from the environmental point of view, but also from a socioeconomic perspective [1]. Soil
45 surface characteristics (SSC), such as moisture (*mv*), roughness, texture, and slaking crusts are some
46 key variables used to understand and model natural hazards, such as erosion, drought, runoff, and
47 floods [2]. Particularly, soil moisture and roughness are important variables in land surface
48 hydrology as they control the amount of water that infiltrates into the soil and replenishes the water
49 table [3]. Synthetic Aperture Radar (SAR) data were widely and successfully used for monitoring
50 the spatial and temporal evolution of soil moisture and roughness [4–7]. The estimation of soil
51 moisture and roughness was performed by inverting the measured SAR backscatter through SAR
52 backscattering models (both empirical and physical). Unlike physical models, empirical models
53 need to be calibrated using site specific *in situ* measurements and SAR observation at each time are
54 used over a different study area. Moreover, the validity domain of semi-empirical models is limited
55 to the range of data used for calibration. The most commonly empirical models are the models of
56 Oh [8–11] and Dubois [12]; while, the most popular physical models are Integral equation model
57 (IEM) [13], IEM calibrated by Baghdadi, called in this paper "IEM_B" [14–19], and Advanced
58 Integral Equation Model (AIEM) [20].

59 For bare soils, SAR backscattering models allow backscattering coefficients simulation by using
60 soil parameters (mainly dielectric constant, and roughness) and SAR configurations (frequency,
61 incidence angle, polarization) as input. Several studies reported important discrepancies between
62 backscattering models simulations and SAR observations [15,21–23]. The discrepancy between SAR
63 simulations and SAR measurements is mainly related to the description of surface roughness which
64 is an important input to SAR backscattering models [17,24,25]. For most of the backscattering
65 models the surface roughness is described by three parameters: the standard deviation of the height
66 (*Hrms*), the correlation length (*L*) and the shape of the correlation function [13,26]. The correlation
67 length is usually measured with an uncertainty which introduces an error on simulated
68 backscattering coefficients [27–33]. A few studies proposed a semi-empirical calibration of SAR
69 backscattering models in order to reduce the uncertainty on SAR simulations [14,15,17–19,34,35]. In
70 [14,15,17–19,34] the method consisted of replacing the measured *L* by a fitting parameter, so-called
71 *Lopt*, which was found to be related to *Hrms* (*Lopt* increases with *Hrms*). *Lopt* is a function of *Hrms*
72 (linear, exponential, or power calibration) which depends on SAR parameters (incidence angle,
73 polarization and frequency). This calibration reduces IEM's input soil parameters (*Hrms* and *mv*
74 instead of *Hrms*, *L* and *mv*). Rahman *et al.* [35] proposed a method for deriving *L* through the IEM.
75 In this method, the radar signal is modeled as a function of only *Hrms* and *L* and the contribution of
76 soil moisture on backscattering coefficients is ignored (dry soil). Thus, *L* could be estimated by
77 inverting the IEM.

78 Several studies have been carried out to evaluate and compare the robustness of the
79 backscattering models such as, Oh, Dubois and IEM (original IEM, IEM_B and AIEM). Zribi *et al.*
80 [23] evaluated the Oh model and IEM using L-, C- and X-bands SAR data and *in situ*
81 measurements. Results showed that the IEM provides accurate simulations (RMSE about 2.0 dB)
82 only over smooth surfaces. In addition, for rough surfaces and medium incidence angle, Oh model
83 simulations retrieve backscattering values very close to the measured ones, while showing poor
84 correlation with measured backscattering coefficients over smooth areas. Baghdadi and Zribi [21]
85 evaluated the backscattering models IEM, Oh and Dubois by using large C-band SAR data and *in situ*
86 measurements. Results showed that these models frequently tend to over-estimate or under-
87 estimate the radar signal (in the order of -3.0 dB) and the errors on model simulation depends on
88 height surface roughness, *Hrms*, soil moisture, *mv*, and/or incidence angle. Baghdadi *et al.* [18]
89 evaluated the potential of IEM, Oh and Dubois models by using TerraSAR-X images acquired over
90 France and Tunisia and experimental datasets of *in-situ* measurements (*mv* ranged between 5 vol.%
91 and 41 vol.% and *Hrms* between 0.42 cm and 4.55 cm). In this case, the semi-empirical Oh model
92 correctly simulated the backscattering (showing over or under-estimation of the backscatter < 1dB,
93 and RMSE < 3dB), while Dubois model showed a poor correlation between real data and
94 simulations, with RMSE between 2.2 and 4.4 dB and over or under-estimation of the backscatter of

95 about 3.4 dB. In addition, the IEM simulates correctly the backscattering at X-band for $H_{rms} < 1.5$ cm
96 by using the exponential correlation function and for $H_{rms} > 1.5$ cm by using the Gaussian
97 correlation function. Panciera *et al.* [36] compared the performances of the IEM, Dubois and Oh
98 models by using fully polarized L-band airborne data (incidence angles between 24° and 38°) and in-
99 situ measurements (mv between 5 vol.% and 39 vol.% and H_{rms} between 1cm and 7.6 cm) acquired
100 over the study area in southeastern Australia. At HH polarization, the three models simulated the
101 backscattering with almost similar accuracy, showing a mean error between the simulated and the
102 observed backscattering coefficients of about 1.6 dB in absolute value (standard deviation "std"
103 about ± 2.5 dB). At VV polarization, the Oh model resulted to be more accurate than IEM and Dubois
104 models: the mean errors between the simulated and observed backscattering were equal to 4.5 dB
105 (std = ± 2.0 dB), 1.7 dB (std = ± 2.3 dB), and -0.4 dB (std = ± 2.4 dB) for IEM, Dubois, and Oh model,
106 respectively.

107 Several studies confirmed that the use of the calibrated correlation length, as proposed by
108 Baghdadi *et al.* [14–19] is able to improve the performance of the IEM at both both HH and VV
109 polarizations [36–38]. Dong *et al.* [37] used the calibrated correlation length in the AIEM to simulate
110 SAR data in C-band. Results showing that the RMSE reduced from 3.1 to 1.7 dB at HH and VV
111 polarizations and from 31.0 to 5.1 dB at HV polarization. Panciera *et al.* [36] showed that the use of
112 calibrated correlation length decreases the errors on IEM simulation with a bias equal to about -0.3
113 dB (std about ± 1.1 dB) at both HH and VV polarizations.

114 The aim of this study is to evaluate the most popular backscattering SAR models (Oh, Dubois,
115 IEM, IEM_B, and AIEM) by using a wide range of SAR data and in-situ measurements. With the
116 arrival of Sentinel-1A and -1B satellites that provides free high resolution SAR data with 3 days
117 revisit time, several research teams work actually on developing methods for mapping soil
118 moisture using these Sentinel-1 data. Most of methods for soil moisture mapping are based on
119 using backscattering models for soil moisture estimates. The objective of our study is to evaluate
120 the most commonly backscattering models using a wide dataset of SAR data and in situ
121 measurements acquired over numerous agricultural sites in France, Italy, Germany, Belgium,
122 Luxembourg, Canada and Tunisia. Thus, this study could be of a great importance for scientific
123 community since it help on understand backscattering models accuracy and performance for wide
124 range of soil surface conditions, acquired for several study areas through the world by numerous
125 SAR sensors. Never before have been evaluated all these backscatter models together in the same
126 literature with such a wide dataset. These wide ranges of data using all these models together in the
127 same literature. In addition, this study is the first that evaluates the AIEM backscatter models using
128 L-, C- and X- bands together. A description of the study areas and different datasets used in this
129 study is provided in Section 2. Section 3 the models are described. The results are shown in section
130 4. Finally, section 5 presents the conclusion.

Mis en forme : Surlignage

131 2. Dataset

132 2.1. Study areas

133 A wide range of datasets composed of AIRSAR, SIR-C, JERS-1, PALSAR-1, ESAR, ERS,
134 RADARSAT, ASAR and TerraSAR-X acquisitions over numerous agricultural sites in France, Italy,
135 Germany, Belgium, Luxembourg, Canada and Tunisia (Table 1), have been used in this research
136 work. In addition, in-situ measurements of soil moisture and surface roughness were carried out
137 simultaneously to SAR acquisitions over bare soil surfaces.

138 2.2. Satellite data

139 A large number of L-, C- and X-band images (approximately 1.25 GHz, 5.3 GHz and 9.6 GHz,
140 respectively) were acquired between 1994 and 2014 with different incidence angles (between 18°
141 and 57°) and in HH, VV and HV polarizations (Table 1). The spatial resolution of SAR images is
142 between 1m and 30m (Table 1). Images were first radiometrically calibrated to enable the extraction

143 of the backscattering coefficients (σ°). Then, the mean backscattering coefficients were computed
 144 from calibrated SAR images by linearly averaging the σ° values of all pixels within the plot.

145 2.3. Field data

146 Field measurements of soil moisture and surface roughness have been collected from the bare
 147 plots/fields selected over of the study/test areas. Each plot is a homogeneous surface (similar soil type,
 148 moisture content and surface roughness) of around one hectare or more. In-situ measurements of soil
 149 moisture (*mv*, in vol.%) were carried out for a soil layer of 5 cm or 10 cm in each reference plot by
 150 using both the gravimetric method or a calibrated TDR (time domain reflectometry) probe. For each
 151 bare soil reference field the average soil moisture (*mv*) of all samples was calculated. The soil
 152 moisture ranged between 2 vol.% and 47 vol.%.

153 Roughness measurements were carried out by using laser or needle profilometers (mainly 1 m
 154 and 2 m long, and with 1 cm and 2 cm sampling intervals); while for some in-situ measurement
 155 campaigns, a meshboard technique was used. Several roughness profiles along and across the
 156 direction of tillage were acquired in each reference field. The standard deviation of surface heights
 157 (*Hrms*) and the correlation length (*L*) were calculated by using the mean of all experimental
 158 correlation functions. In our dataset, *Hrms* ranged from 0.2 cm to 9.6 cm and the *L* from 1.2 cm to
 159 38.5 cm.

160 A total of 2442 experimental data of soil moisture content and surface roughness were
 161 available, together with the corresponding values of backscattering coefficient, of which 1262 at HH
 162 polarization, 790 at VV polarization, and 390 at HV polarization (see Table 1).

163 **Table 1.** Description of the dataset used in this study. "Fr": France, "It": Italy, "Ge":
 164 Germany, "Be": Belgium, "Lu": Luxembourg, "Ca": Canada, "Tu": Tunisia.

Site	SAR sensor	Spatial resolution	Freq	Year	Number of data
Orgeval (Fr) [39]	SIR-C	30m x 30m	L	1994	➤ HH : 1262 measurements – 66 in L-band
Orgeval (Fr) [39], [40], [41]	SIR-C, ERS, ASAR	30m x 30m	C	1994; 1995; 2008; 2009;	– 766 in C-band – 430 in X-band
Orgeval (Fr) [41]	PALSAR-1	30m x 30m	L	2009	➤ VV : 790 measurements
Orgeval (Fr) [42]	TerraSAR-X	1m x 1m	X	2008, 2009, 2010	– 159 in L-band – 411 in C-band – 220 in X-band
Pays de Caux (Fr) [43], [44]	ERS; RADARSAT	30m x 30m	C	1998; 1999	– 220 in X-band
Villamblain (Fr) [6], [34], [45]	ASAR	30m x 30m	C	2003; 2004; 2006	➤ HV : 390 measurements – 13 in L-band
Thau (Fr) [47]	RADARSAT TerraSAR-X	30m x 30m 1m x 1m	C X	2010; 2011 2010	– 313 in C-band – 64 in X-band
Touch (Fr) [6], [47]	ERS-2; ASAR	30m x 30m	C	2004; 2006; 2007	
Mauzac (Fr) [46]	TerraSAR-X	1m x 1m	X	2009	
Garons (Fr) [46]	TerraSAR-X	1m x 1m	X	2009	
Kairouan (Tu) [48]	ASAR	30m x 30m	C	2012	
Yzerons (Fr) [50]	TerraSAR-X	1m x 1m	X	2009	
Versailles (Fr) [46]	TerraSAR-X	1m x 1m	X	2010	

Mis en forme : Surlignage

Mis en forme : Surlignage

Seysse (Fr) [46]	TerraSAR-X	1m x 1m	X	2010
Chateauguay (Ca) [43]	RADARSAT	30m x 30m	C	1999
Brochet (Ca) [43]	RADARSAT	30m x 30m	C	1999
Alpilles (Fr) [43]	ERS; RADARSAT	30m x 30m	C	1996; 1997
Sardaigne (It) [51]	ASAR; RADARSAT	30m x 30m	C	2008; 2009
Matera (It) [52]	SIR-C	30m x 30m	L	1994
Alzette (Lu) [35],[30]	PALSAR-1	30m x 30m	L	2008
Dijle (Be) [30]	PALSAR-1	30m x 30m	L	2008; 2009
Zwalm (Be) [30]	PALSAR-1	30m x 30m	L	2007
Demmin (Ge) [30]	ESAR	2m x 2m	L	2006
Montespertoli (It) [36],[53]	AIRSAR	30m x 30m	L	1991

165

166 3. Description of the backscattering models

167 3.1. The semi-empirical Dubois model

168 Dubois *et al.* [12] proposed a semi-empirical model for simulating the backscattering
 169 coefficients in HH and VV polarizations (σ°_{HH} and σ°_{VV}) on bare soils. The expression of σ°_{HH} and
 170 σ°_{VV} depends on the incident angle (θ), the soil dielectric constant (ϵ , which is a function of the soil
 171 moisture content), the soil roughness defined by the standard deviation of surface height ($Hrms$),
 172 and the radar wavelength ($\lambda=2\pi/k$ where k is the wave number). The model optimized for bare soils
 173 according to the validity domain defined by $k Hrms \leq 2.5$, $mv \leq 35$ vol.%, and $\theta \geq 30^\circ$ is expressed as:
 174

$$\sigma^0_{HH} = 10^{-2.75} \left(\frac{\cos^{1.5} \theta}{\sin^5 \theta} \right) 10^{0.026 \tan \theta} (k Hrms \sin \theta)^{1.4} \lambda^{0.7} \quad (1)$$

$$\sigma^0_{VV} = 10^{-2.35} \left(\frac{\cos^3 \theta}{\sin^3 \theta} \right) 10^{0.046 \tan \theta} (k Hrms \sin \theta)^{1.1} \lambda^{0.7}$$

175

176 where θ is expressed in radians and λ in cm, and σ^0_{HH} and σ^0_{VV} are expressed in linear units.

177 3.2. The semi-empirical Oh model

178 Oh *et al.* [8–11] developed between 1992 and 2004 several versions of a semi empirical
 179 backscattering model. Basing on theoretical models, scatterometer measurements and airborne SAR
 180 observations, the Oh model is built over a wide variety of bare soil surfaces. The Oh model relates
 181 the co-polarized ratio p ($=\sigma^{\circ}_{HH}/\sigma^{\circ}_{VV}$) and the cross-polarized ratio q ($=\sigma^{\circ}_{HV}/\sigma^{\circ}_{VH}$) to incident angle
 182 (θ), wave number (k), standard deviation of surface height ($Hrms$), correlation length (L), and soil
 183 moisture (mv) or dielectric constant (ϵ_r).

184 The initial version of the Oh model [9] is defined as:
 185

$$p = \frac{\sigma_{HH}^0}{\sigma_{VV}^0} = \left[1 - \left(\frac{\theta}{90} \right)^{1/3\Gamma_0} \cdot e^{-k Hrms} \right]^2 \quad (2)$$

186

$$q = \frac{\sigma_{HV}^0}{\sigma_{VV}^0} = 0.23 \sqrt{\Gamma_0} (1 - e^{-k Hrms}) \quad (3)$$

187 Where:
188

$$\Gamma_0 = \left| \frac{1 - \sqrt{\epsilon_r}}{1 + \sqrt{\epsilon_r}} \right|^2 \quad (4)$$

189

190

191 Oh *et al.* [10] proposed a new expression for q to incorporate the effect of the incidence angle:

192

$$q = \frac{\sigma_{HV}^0}{\sigma_{VV}^0} = 0.25 \sqrt{\Gamma_0} (0.1 + \sin^{0.9} \theta) (1 - e^{-[1.4-1.6\Gamma_0]k Hrms}) \quad (5)$$

193

194 Oh *et al.* [11] again modified the expressions for p and q , and the following expression for the cross-polarized backscatter coefficient was proposed:

196

$$p = \frac{\sigma_{HH}^0}{\sigma_{VV}^0} = 1 - \left(\frac{\theta}{90} \right)^{0.35mv^{-0.65}} \cdot e^{-0.4(k Hrms)^{1.4}} \quad (6)$$

$$q = \frac{\sigma_{HV}^0}{\sigma_{VV}^0} = 0.1 \left(\frac{Hrms}{L} + \sin 1.3\theta \right)^{1.2} (1 - e^{-0.9(k Hrms)^{0.8}}) \quad (7)$$

$$\sigma_{HV}^0 = 0.11 mv^{0.7} \cos^{2.2} \theta (1 - e^{-0.32(k Hrms)^{1.8}}) \quad (8)$$

197 Oh and Kay [56] demonstrated that the measurement of the correlation length is not accurate
198 and that the ratio q is not sensitive to the roughness parameter (defined as $Hrms/L$). Thus, Oh [8]
199 proposed a new equation for q that ignores the correlation length (L):

$$q = \frac{\sigma_{HV}^0}{\sigma_{VV}^0} = 0.095 (0.13 + \sin 1.5\theta)^{1.4} (1 - e^{-1.3(k Hrms)^{0.9}}) \quad (9)$$

200 The Oh model [8] is optimized for bare soils in the following validity domain:
201 $0.13 \leq kHrms \leq 6.98$, $4 \leq mv$ (vol.%) ≤ 29.1 , and $10^\circ \leq \theta \leq 70^\circ$.

202 The estimation of soil moisture and surface roughness from Oh model requires two
 203 backscattering coefficients at least, with one co-polarized coefficient ($\sigma^{\circ_{HH}}$ or $\sigma^{\circ_{VV}}$) and one cross-
 204 polarized coefficient ($\sigma^{\circ_{HV}}$ or $\sigma^{\circ_{VH}}$). The availability of $\sigma^{\circ_{VV}}$ and $\sigma^{\circ_{VH}}$ allows using the ratio q and
 205 $\sigma^{\circ_{HV}}$ in the inversion process of SAR data, while the ratio p/q , as well as $\sigma^{\circ_{HV}}$, is used in the case
 206 where SAR data are available in the both HH and HV polarizations.

207 3.3. The physical Integral Equation Model (IEM)

208 The Integral Equation IEM is a physical model [13], where the soil is characterized by the
 209 dielectric constant (ϵ_r), the standard deviation of surface height ($Hrms$), the form of the correlation
 210 function, and the correlation length (L). The IEM also takes into account the sensor parameters such
 211 as the incidence angle (θ), the polarization (pq with $p,q=H$ or V), and the radar wave number ($k=2\pi/\lambda$
 212 where λ is the wavelength). The IEM has a validity domain that covers the range of roughness
 213 values that are commonly encountered for agricultural surfaces:

$$kHrms \leq 3$$

$$\left((k Hrms \cos \theta)^2 / \sqrt{0.46k L} \right) \exp \left\{ -\sqrt{0.92k L(1 - \sin \theta)} \right\} < 0.25 \quad (10)$$

214 Over bare soils in agricultural areas, the backscattering coefficient of the surface contribution
 215 is expressed at HH and VV polarizations as:

$$\begin{aligned} \sigma_{pp}^{\circ} &= \frac{k^2}{2} |f_{pp}|^2 e^{-4k^2 Hrms^2 \cos^2 \theta} \sum_{n=1}^{+\infty} \frac{(4k^2 Hrms^2 \cos^2 \theta)^n}{n!} W^{(n)}(2k \sin \theta, 0) \\ &+ \frac{k^2}{2} \operatorname{Re}(f_{pp}^* F_{pp}) e^{-3k^2 Hrms^2 \cos^2 \theta} \sum_{n=1}^{+\infty} \frac{(4k^2 Hrms^2 \cos^2 \theta)^n}{n!} W^{(n)}(2k \sin \theta, 0) \\ &+ \frac{k^2}{8} |F_{pp}|^2 e^{-2k^2 Hrms^2 \cos^2 \theta} \sum_{n=1}^{+\infty} \frac{(k^2 rms^2 \cos^2 \theta)^n}{n!} W^{(n)}(2k \sin \theta, 0) \end{aligned} \quad (11)$$

216 At cross polarization, the backscattering coefficient is as follows:

217

$$\sigma_{hv}^{\circ} = \frac{k^2}{16\pi} e^{-2k^2 Hrms^2 \cos^2 \theta} \sum_{n=1}^{+\infty} \sum_{m=1}^{+\infty} \frac{(k^2 Hrms^2 \cos^2 \theta)^{n+m}}{n!m!} \quad (12)$$

$$\iint \left[|F_{hv}(u, v)|^2 + F_{hv}(u, v) F_{hv}^*(-u, -v) \right] W^{(n)}(u - k \sin \theta, v) W^{(m)}(u + k \sin \theta, v) du dv$$

218 Where:

$$f_{hh} = \frac{-2R_h}{\cos \theta}; f_{vv} = \frac{2R_v}{\cos \theta} \quad (13)$$

$$R_h = \frac{\mu_r \cos \theta - \sqrt{\mu_r \epsilon_r - \sin^2 \theta}}{\mu_r \cos \theta + \sqrt{\mu_r \epsilon_r - \sin^2 \theta}} : \text{Fresnel coefficient at horizontal polarization} \quad (14)$$

$$R_v = \frac{\epsilon_r \cos \theta - \sqrt{\mu_r \epsilon_r - \sin^2 \theta}}{\epsilon_r \cos \theta + \sqrt{\mu_r \epsilon_r - \sin^2 \theta}} : \text{Fresnel coefficient at vertical polarization} \quad (15)$$

$$F_{hh} = 2 \frac{\sin^2 \theta}{\cos \theta} \left[4R_h - \left(1 - \frac{1}{\varepsilon_r} \right) (1 + R_h)^2 \right] \quad (16)$$

$$F_{vv} = 2 \frac{\sin^2 \theta}{\cos \theta} \left[\left(1 - \frac{\varepsilon_r \cos^2 \theta}{\mu_r \varepsilon_r - \sin^2 \theta} \right) (1 - R_v)^2 + \left(1 - \frac{1}{\varepsilon_r} \right) (1 + R_v)^2 \right] \quad (17)$$

$$F_{hv}(u, v) = \frac{uv}{k \cos \theta} \left[\frac{8R^2}{\sqrt{k^2 - u^2 - v^2}} + \frac{-2 + 6R^2 + \frac{(1+R)^2}{\varepsilon_r} + \varepsilon_r(1-R)^2}{\sqrt{\varepsilon_r k^2 - u^2 - v^2}} \right] \quad (18)$$

$$R = \frac{R_v - R_h}{2} \quad (19)$$

219 ε_r : dielectric constant, obtained on the basis of volumetric water content (mv). In our study,
220 Hallikainen empirical model is used [57].

221 μ_r : relative permittivity

222 Re: real part of the complex number

223 f_{pp}^* : conjugate of the complex number f_{pp}

224 $W^{(n)}$ is the Fourier transform of the n^{th} power of the surface correlation $\rho(x, y)$
225 function:

$$W^{(n)}(a, b) = \frac{1}{2\pi} \iint \rho^n(x, y) e^{-i(ax+by)} dx dy \quad (20)$$

226 The distribution of $\rho(x, y)$ is exponential for low surface roughness values and Gaussian
227 for high surface roughness values. For one-dimensional roughness profiles, the correlation
228 functions are defined as follows:

$$\begin{aligned} \rho(x) &= e^{-\left(\frac{x}{L}\right)} & : & \text{exponential} \\ &= e^{-\left(\frac{x}{L}\right)^2} & : & \text{Gaussian} \end{aligned} \quad (21)$$

229 3.4. IEM modified by Baghdadi (IEM_B)

230 Several studies reported important discrepancies between backscattering coefficients
231 simulated by IEM and those measured by SAR sensors [36,44,49,58–62]. Baghdadi *et al.* [14,28]
232 showed that the discrepancy between the observed and IEM simulated backscattering coefficients is
233 mainly due to the correlation length parameter which is difficult to be measured with a good
234 accuracy. To reduce such incongruities between simulated and measured backscattering values,
235 Baghdadi *et al.* [34,46,63,64] proposed a semi-empirical calibration of the IEM backscattering, which
236 consists of replacing the *in situ* measured correlation length by a fitting parameter ($Lopt$). $Lopt$
237 depends on surface roughness conditions and SAR configurations (incidence angle, polarization
238 and radar wavelength). This calibration has been performed by using large experimental datasets
239 and SAR configurations (incidence angles from 23° to 57°, and HH, HV, and VV polarizations), and

240 it has been carried separately at X-band in [46], C-band in [17,34] and L-band in [64]. The proposed
 241 calibration reduces the IEM's input soil parameters from three to two (*Hrms* and *mv* only, instead of
 242 *Hrms*, *L* and *mv*).

243 *Lopt* is computed at L-, C-, and X-bands using a Gaussian correlation function and it is
 244 described as follows:
 245

$$\text{In X-band: } \begin{cases} \text{Lopt} (Hrms, \theta, HH) = 18.102 e^{-1.891\theta} Hrms^{0.7644e^{0.2005\theta}} \\ \text{Lopt} (Hrms, \theta, VV) = 18.075 e^{-2.1715\theta} Hrms^{1.2594e^{-0.8308\theta}} \end{cases} \quad (22)$$

246

$$\text{In C-band: } \begin{cases} \text{Lopt} (Hrms, \theta, HH) = 0.162 + 3.006 (\sin 1.23 \theta)^{-1.494} Hrms \\ \text{Lopt} (Hrms, \theta, HV) = 0.9157 + 1.2289 (\sin 0.1543 \theta)^{-0.3139} Hrms \\ \text{Lopt} (Hrms, \theta, VV) = 1.281 + 0.134 (\sin 0.19 \theta)^{-1.59} Hrms \end{cases} \quad (23)$$

247

$$\text{In L-band: } \begin{cases} \text{Lopt} (Hrms, \theta, HH) = 2.6590 \theta^{-1.4493} + 3.0484 Hrms \theta^{-0.8044} \\ \text{Lopt} (Hrms, \theta, VV) = 5.8735 \theta^{-1.0814} + 1.3015 Hrms \theta^{-1.4498} \end{cases} \quad (24)$$

248

249 Where θ is in radians; *Lopt* and *Hrms* are in centimeters. Several studies showed that the use of
 250 the fitting parameter *Lopt* allows more correct estimations of the radar backscattering coefficient
 251 [51].

252 3.5. The Advanced Integral Equation Model

253 The Advanced Integral Equation Model (AIEM) [20] is the updated version of the Integral
 254 Equation Model (IEM) [65]. In a comparison with the IEM, two improvements have been integrated
 255 into the AIEM: 1) the complete expressions for the Kirchhoff field coefficient and the
 256 complementary field coefficient based on the removal of the simplification assumption of the
 257 Green's function have been included in the AIEM [20] and 2) a continuous Fresnel reflection
 258 coefficient is obtained using a transition model [66]. This update allows a more precise calculation
 259 of the simple scattering for a surface with a wide range of dielectric constant (ϵ_r), large standard
 260 deviation of heights *Hrms*, and various remote sensing configurations. The AIEM simulates the
 261 radar backscattering coefficients basing on the same parameters as the IEM.

262 4. Results and discussion

263 This section shows the evaluation results of the five radar backscattering models Dubois, Oh,
 264 IEM, IEM_B and AIEM using large datasets, characterized by various radar wavelength (L,C and
 265 X), wide range of incidence angles and large geographical distribution in regions with different
 266 climate conditions (humid, semi-arid and arid sites). In this study each plot is considered as
 267 sampling unit. For each plot, SAR data was simulated through `backscatter_models` using in situ
 268 measurements (*mv*, *Hrms* and *L*) averaged within that plot. Then, the simulated SAR signal were
 269 compared with the backscattering coefficients computed from calibrated SAR images by linearly
 270 averaging the σ^0 values of all pixels within the plot.

271 4.1. Evaluation of the Dubois model

272 The evaluation of Dubois model was carried out for different scenarios using all data, per
 273 radar wavelength, and by range of soil moisture, *k Hrms*, and incidence angle.

274 Using all data, the Dubois model over-estimates slightly the radar signal by about 1.0 dB in
 275 HH polarization and under-estimates slightly the radar signal by about 0.7 dB in VV polarization
 276 (Table 2 Figures 1 and 2). RMSE is about 4.0 dB and 2.9 dB at HH and VV polarization, respectively
 277 (Table 2). The analysis of the error according to each radar frequency band separately (L, C and X)

278 shows an over-estimation in HH polarization, which is almost the same at L-, C- and X-bands
279 (between 0.9 dB and 1.1 dB). In VV polarization, the Dubois model under-estimates the radar signal
280 by about 1.8 dB and 0.4 dB for X and C bands, respectively. For L band, the Dubois model fits
281 correctly the radar signal in VV because the difference between real data and simulations is about
282 0.2 dB. The RMSE in HH is the same as at X- and C-bands, and is about 4.1 dB and decreases to 3.0
283 dB at L-band. In VV polarization, the RMSE increases with the radar frequency (2.5 dB at L-band,
284 2.8 dB at C-band and 3.1 dB at X-band).

285 The analysis of the error of the Dubois model according to the validity domain was studied by
286 range of surface roughness ($kHrms$), soil moisture (mv) and incidence angle (Table 2). The Dubois
287 model underestimates the radar signal for $kHrms < 2.5$ (validity domain of the Dubois model) by
288 about 0.4 dB and 1.2 dB in HH and VV polarizations, respectively. In the case of $kHrms < 2.5$, the
289 RMSE is about 3.6 and 3.0 dB for HH and VV polarizations, respectively. In addition, the Dubois
290 model overestimates the radar signal for $kHrms > 2.5$ by about 2.9 dB in HH polarization with RMSE
291 about 4.6 dB. In VV polarization, the Dubois model fits correctly the radar signal in the case of
292 $kHrms > 2.5$ with a difference between real and simulated data of about 0.2 dB and a RMSE of 2.5 dB
293 (Table 2).

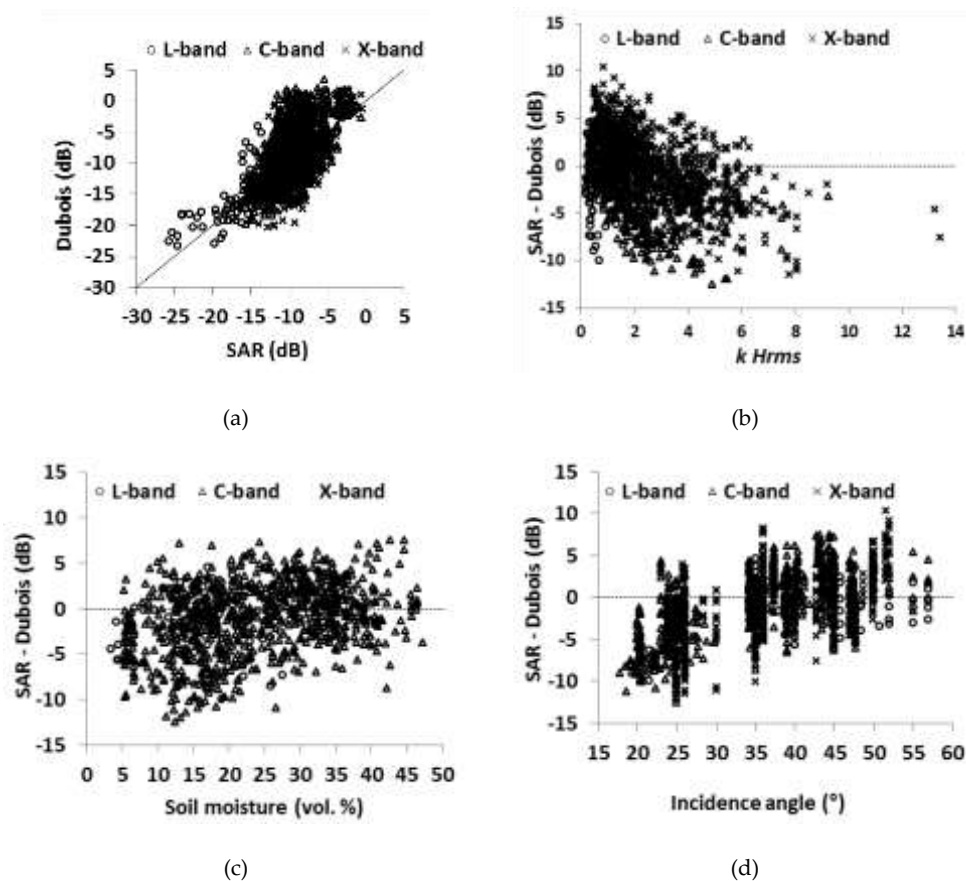
294 Moreover, the evaluation of the Dubois model was carried out by range of soil moisture (mv).
295 Results show an overestimation in HH pol. by about 2.6 dB and a slightly underestimation in VV by
296 about 0.5 dB with mv -values lower than 20 vol.% (RMSE= 4.6 and 2.8 dB at HH and VV,
297 respectively) (Table 2). In besides, the Dubois model correctly simulates the backscattering
298 coefficient in HH pol. with a difference between real data and simulations about 0.3 dB and
299 underestimates the radar signal in VV by about 1.0 dB with mv -values greater than 20 vol.%. In the
300 case of mv -values greater than 20 vol.%, the RMSE is about 3.4 dB and 3.0 dB for HH and VV
301 polarization respectively. Finally, the performance of Dubois model was studied according to
302 ranges of incidence angle (Table 2). For $\theta < 30^\circ$ (outside the validity domain of the Dubois model),
303 the Dubois model overestimates the radar signal by -4.2 dB in HH polarization (RMSE=5.5 dB) and
304 slightly underestimates the radar signal in VV polarization (real data – simulations = -0.6 dB) with a
305 RMSE of 2.9 dB. At $\theta > 30^\circ$, the Dubois model correctly simulates the backscattering coefficient in
306 HH pol. with a difference between real data and model of 0.3 dB at HH polarization and
307 underestimates the backscattering at VV pol. by about 1.5 dB (RMSE= 3.2 dB and 2.9 dB for HH
308 and VV polarizations, respectively).

309

310
311
312

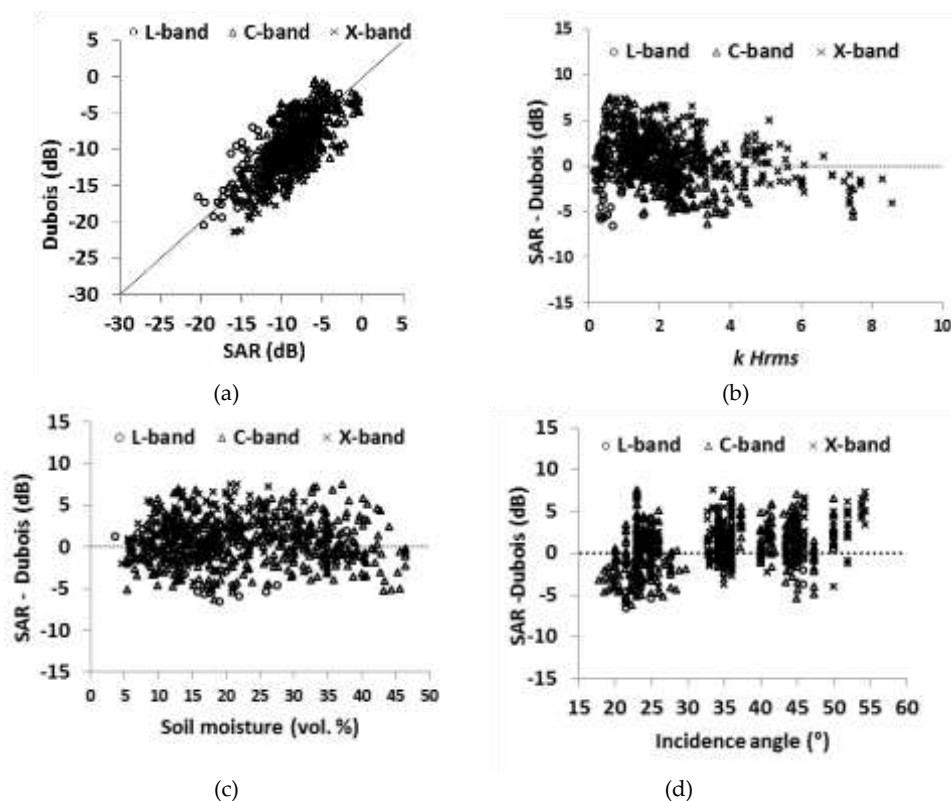
Table 2. Comparison between the Dubois model output and real data using the entire dataset, and by separating two intervals of *kHrms*, soil moisture (*mv*) and incidence angle (θ). Bias = real data – simulations.

		All data	L-band	C-band	X-band	<i>kHrms</i> < 2.5	<i>kHrms</i> > 2.5	<i>mv</i> < 20 vol. %	<i>mv</i> > 20 vol. %	θ < 30°	θ > 30°
Dubois for HH pol.	Bias (dB)	-1.0	-1.0	-1.1	-0.9	+0.4	-2.9	-2.6	+0.3	-4.2	+0.3
	RMSE (dB)	4.0	3.0	4.1	4.1	3.6	4.6	4.6	3.4	5.5	3.2
Dubois for VV Pol.	Bias (dB)	+0.7	-0.2	+0.4	+1.8	+1.2	-0.2	+0.5	+1.0	-0.6	+1.5
	RMSE (dB)	2.9	2.5	2.8	3.1	3.0	2.5	2.8	3.0	2.9	2.9



313
314
315
316
317

Figure 1. Comparison between backscattering coefficient values obtained from SAR images and those estimated from the Dubois model at HH polarization. (a): Dubois model simulations vs SAR data, (b): difference between SAR signal and the Dubois model vs soil roughness (*kHrms*), (c): difference between SAR signal and the Dubois model vs soil moisture (*mv*), (d): difference between SAR signal and Dubois model vs incidence angle.



318 **Figure 2.** Comparison between backscattering coefficient values obtained from SAR images and those
 319 estimated using the Dubois model at VV polarization. (a): Dubois model simulations vs SAR data, (b):
 320 difference between SAR signal and Dubois model vs soil roughness ($kHrms$), (c): difference between SAR
 321 signal and the Dubois model vs soil moisture (mv), (d): difference between SAR signal and the Dubois model
 322 vs incidence angle.

323 4.2. Evaluation of the Oh model

324 The Oh model versions developed in 1992, 1994, 2002 and 2004 were applied to our datasets.
 325 The evaluation of the different Oh model versions was carried out firstly using all data, successively
 326 for each radar wavelength (L, C and X bands), and finally by range of soil moisture, $kHrms$ and
 327 incidence angle (Table 3, Figures 3, 4 and 5).

328 Using the entire dataset, results showed that the different versions of Oh model correctly
 329 simulate the backscattering at both HH and VV polarizations with difference between real data and
 330 simulations varying between -0.9 and +0.4 dB at HH pol. and between (-1.3 dB and +0.4 dB) in VV
 331 pol. The RMSE values are approximately the same for all models and in both HH and VV
 332 polarizations, i.e. between 2.4 dB and 2.8 dB. The Oh 1992 model simulates slightly better the
 333 backscattering than the other versions (Table 3). For HV polarization, the Oh 2002 model simulates
 334 correctly the backscattering with a difference between real and simulated data of about +0.7 dB,
 335 with RMSE equal to 2.9 dB.

336 In L-band, the different versions of the Oh model underestimate the backscattering at both HH
 337 and VV polarizations. This underestimation varies between 1.3 dB and 2.5 dB in HH polarization
 338 and between 0.7 dB and 2.1 dB in VV polarization (table 3). The RMSE is slightly higher in HH than
 339 in VV polarization (between 2.8 dB and 3.7 dB in HH and between 2.6 dB and 3.4 dB in VV). The Oh
 340 1994 version better simulates the backscattering than other versions of Oh model, with an
 341 underestimation of the backscattering between 1.3 dB and 0.7 dB and RMSE of 2.8 and 2.6 dB for
 342 HH and VV polarizations, respectively. At HV polarization, the Oh model underestimates the
 343 backscattering by about 1.5 dB with RMSE equal to 3.1 dB.

344 In C-band, the Oh 1992 model correctly simulates the backscattering in both HH and VV
345 polarizations with differences between real and simulated data of 0.1 dB and 0.4 dB at HH and VV
346 polarizations, respectively (Table 3). Besides, the RMSE is of 2.4 dB at HH and 2.3 dB at VV pol.
347 Moreover, the other Oh versions overestimate the backscattering in both HH and VV polarizations
348 (between 0.9 dB and 1.5 dB) with similar RMSE between 2.6 dB and 2.8 dB. At HV polarization, the
349 Oh 2002 model slightly underestimates the backscattering by about 1.0 dB with a RMSE of 2.7 dB.

350 The analysis of results obtained in X-band shows that Oh model versions simulate the radar
351 signal with difference between real data and simulations between 0.0 and -1.2 dB in HH and
352 between +0.4 and -2.1 dB in VV (Table 3, Figures 3,4, and 5). The RMSE is between 2.3 and 2.8 dB
353 in HH and between 2.0 and 2.7 dB in VV polarization. For HV polarization, the Oh model over-
354 estimates the backscattering by about 0.9 dB with RMSE of 3.8 dB.

355 The analysis of the error was studied by selecting two ranges of surface roughness ($kHrms < 2.0$
356 and $kHrms > 2.0$) (Table 3). This range is different from the general validity domain of the Oh model
357 ($0.13 \leq kHrms \leq 6.98$) because it covers the entire dataset except only a few points. For $kHrms < 2.0$, the
358 1994, 2002 and 2004 Oh models simulate correctly the backscattering at both HH and VV
359 polarizations with differences between real data and simulations between -0.5 and +0.6 dB and
360 RMSE between 2.4 dB and 2.7 dB. The Oh 1992 model underestimates the backscattering by 1.3 dB
361 and 1.0 dB at HH and VV polarizations, respectively (RMSE is 2.9 for HH pol. and 2.7 dB for VV
362 pol.). For $kHrms > 2.0$, the 1992 and 2002 Oh versions simulate correctly backscattering at both HH
363 and VV polarizations with difference between real and simulated data between -0.5 dB and -1.0 dB
364 with RMSE between 2.3 and 2.6 dB. The 1994 Oh model over-estimates the backscattering at both
365 HH and VV polarizations by about 1.7 dB and 2.1 dB, respectively (RMSE = 2.9 dB). The last version
366 of the Oh model (Oh, 2004) underestimates the backscattering in HH polarization by about 1.5 dB
367 (RMSE = 2.6 dB) and over-estimates it in VV polarization by about 2.0 dB (RMSE= 2.8 dB). At HV
368 polarization, for $kHrms < 2$, the Oh 2002 model underestimates the backscattering in HV by 1.8 dB
369 (RMSE = 2.5 dB). In addition, Oh model correctly fits the backscattering for $kHrms > 2.0$, with a
370 difference between the real and simulated data of about -0.7 dB and RMSE of 2.5 dB.

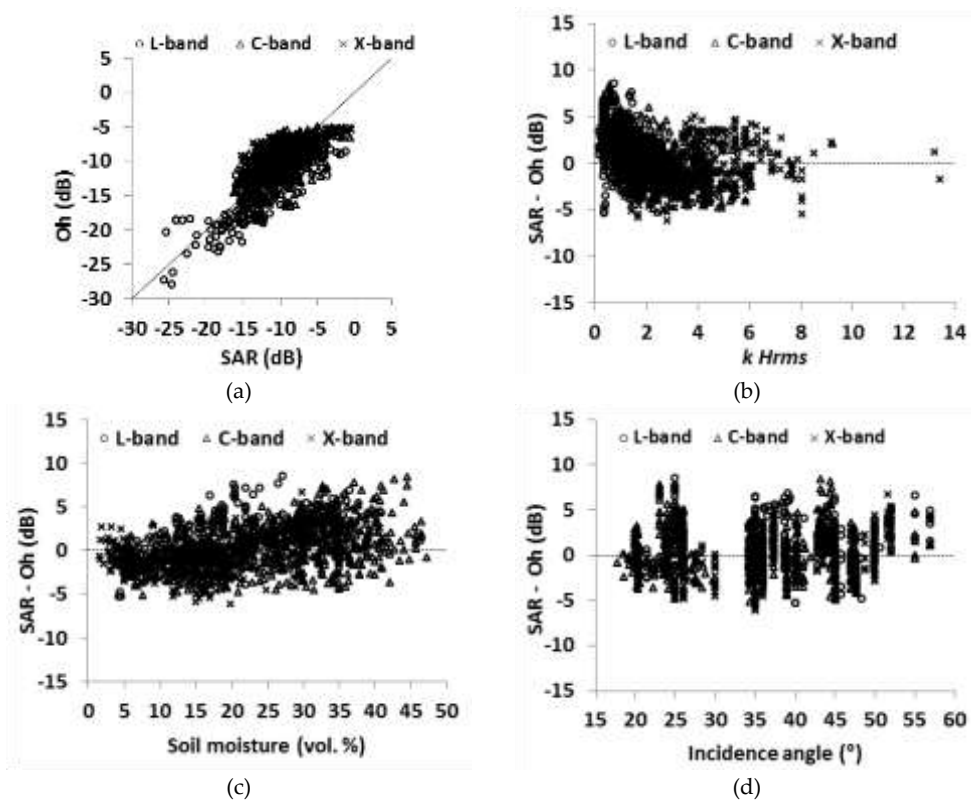
371 Finally, the performance of the Oh model was studied according to its validity domain by
372 selecting two intervals of soil moisture ($mv < 29.1$ and $mv > 29.1$ vol.%). For $mv < 29.1$ vol.%, the 1992
373 and 2002 Oh versions simulate correctly the backscattering coefficient at both HH and VV
374 polarizations with a difference between real and simulated data varying between -0.3 dB and -0.7
375 dB. In addition, the 1994 and 2004 Oh models overestimate the backscattering at both HH and VV
376 polarizations (Table 3) with RMSE between 2.6 dB and 2.9 dB. In conclusion, for $mv < 29.1$ vol.%, the
377 1992 Oh model provides the best simulations. For $mv > 29.1$ vol.%, the 1994, 2002 and 2004 Oh models
378 correctly simulate the backscattering with a difference between real and simulated data between -
379 0.8 dB and +0.5 dB, while the 1992 Oh model underestimates the backscattering by about 1.9 dB and
380 1.5 dB at HH and VV polarizations, respectively (RMSE =3.1 dB for HH and 2.7 dB for VV). The
381 RMSE values are approximately the same in the Oh 1994, 2002 and 2004 versions, and range
382 between 2.2 dB and 2.6 dB. At HV polarization, the Oh model correctly simulates the backscattering
383 for both range of mv -values, with RMSE of 3.0 dB for $mv < 29.1$ vol.% and RMSE of 2.6 dB for
384 $mv > 29.1$ vol.%.

385 The validity domain of Oh model according to the incidence angle ($10^\circ \leq \theta \leq 70^\circ$) covers the
386 entire dataset. Moreover our results showed that the performance of the Oh model is not dependent
387 on the incidence angle.

388 In conclusions, the Oh models simulate correctly the backscattering. Results showed that Oh
389 1992 version is slightly better than other model versions. The performance of Oh model seems to be
390 better in C- and X-bands than L-band. Moreover, most versions of the Oh model correctly simulate
391 the backscattering in most cases although outside its mv validity domain.

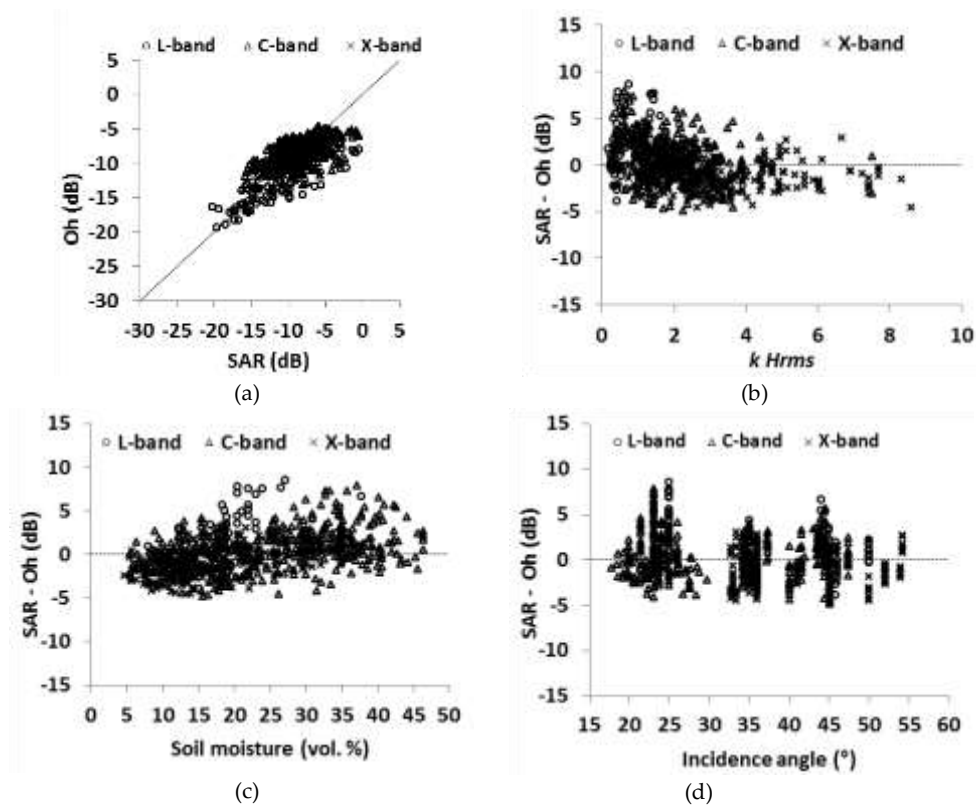
Table 3. Comparison between real data and Oh models for all data and different ranges of kHrms and soil moisture (*mv*). Bias = real data – simulations.

		All data	L-band	C-band	X-band	kHrms < 2.0	kHrms > 2.0	<i>mv</i> < 29.1vol.%	<i>mv</i> > 29.1vol.%	
Oh <i>et al.</i> (1992)	HH	Bias (dB)	+0.4	+2.5	+0.1	0.0	+1.3	-0.5	-0.3	+1.9
		RMSE (dB)	2.6	3.7	2.4	2.5	2.9	2.3	2.3	3.1
	VV	Bias (dB)	+0.1	+2.1	+0.4	-1.2	+1.0	-0.7	-0.4	+1.5
		RMSE (dB)	2.4	3.4	2.3	2.1	2.7	2.0	2.3	2.7
Oh <i>et al.</i> (1994)	HH	Bias (dB)	-0.9	+1.3	-1.2	-1.2	-0.05	-1.7	-1.6	+0.5
		RMSE (dB)	2.8	2.8	2.7	2.8	2.6	2.9	2.9	2.5
	VV	Bias (dB)	-1.3	+0.7	-1.3	-2.1	-0.5	-2.1	-1.7	-0.4
		RMSE (dB)	2.6	2.6	2.6	2.7	2.4	2.9	2.8	2.2
Oh <i>et al.</i> (2002)	HH	Bias (dB)	-0.3	+2.1	-0.9	-1.0	+0.3	-0.9	-0.7	+0.4
		RMSE (dB)	2.7	3.2	2.7	2.8	2.7	2.6	2.7	2.5
	HV	Bias (dB)	+0.7	+1.5	+1.0	-0.9	+1.8	-0.7	+0.5	+0.8
		RMSE (dB)	2.9	3.1	2.7	3.8	3.2	2.5	3.0	2.6
VV	Bias (dB)	-0.6	+1.8	-1.2	+0.4	-0.2	-1.0	-0.7	-0.5	
	RMSE (dB)	2.5	2.9	2.7	2.0	2.5	2.6	2.6	2.5	
Oh (2004)	HH	Bias (dB)	-0.5	+2.1	-1.0	-0.6	0.6	+1.5	-0.9	+0.4
		RMSE (dB)	2.6	3.3	2.7	2.3	2.6	2.6	2.7	2.6
	VV	Bias (dB)	-1.1	+1.4	-1.5	-1.4	-0.2	-2.0	-1.3	-0.8
		RMSE (dB)	2.6	2.8	2.8	2.1	2.4	2.8	2.6	2.6

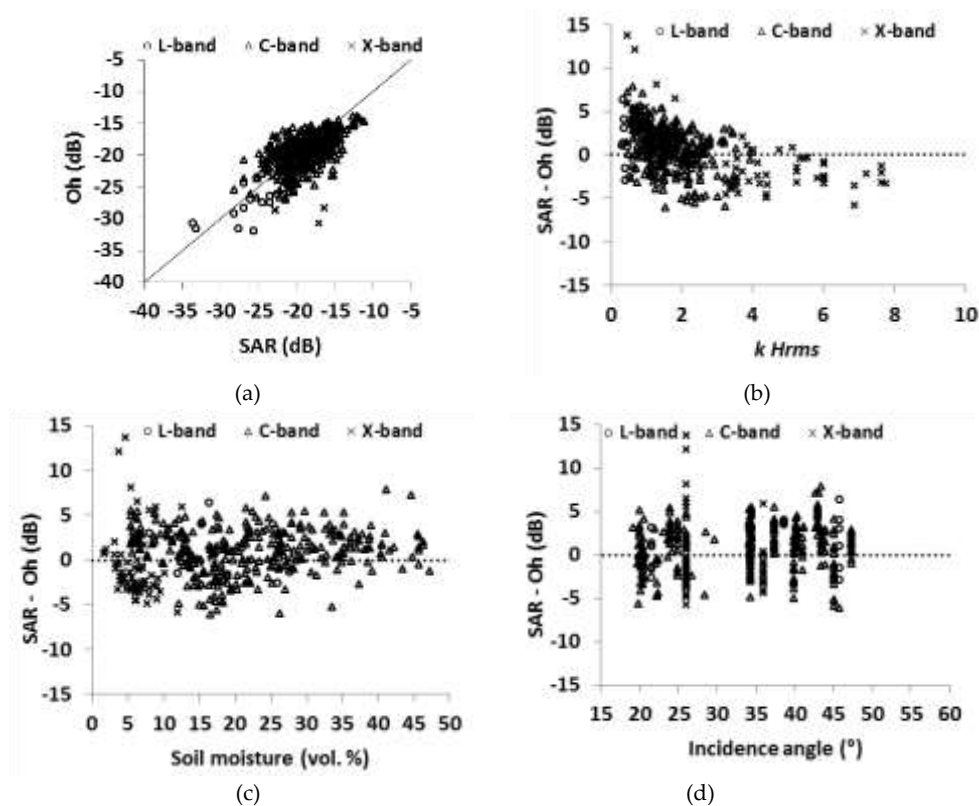


395 **Figure 3.** Comparison between backscattering coefficients derived from SAR images and those
 396 estimated from the Oh 1992 model at HH polarization, (a): Oh model simulations vs SAR data, (b):
 397 difference between SAR signal and Oh model results vs soil roughness ($kHrms$), (c): difference
 398 between SAR signal and Oh model results vs soil moisture (mv), (d): difference between SAR signal
 399 and Oh model results vs incidence angle.

400



401 **Figure 4.** Comparison between backscattering coefficients derived from SAR images and those
 402 estimated from the Oh 1992 model at VV polarization, (a): Oh simulations vs SAR data, (b):
 403 difference between SAR signal and the Oh model vs soil roughness ($kHrms$), (c): difference between
 404 SAR signal and Oh model results vs soil moisture (mv), (d): difference between SAR signal and Oh
 405 model results vs incidence angle.



406 **Figure 5.** Comparison between backscattering coefficients derived from SAR images and those
 407 estimated from the Oh 2002 model at HV polarization, (a): Oh simulations vs SAR data, (b):
 408 difference between SAR signal and Oh model results vs soil roughness ($kHrms$), (c): difference
 409 between SAR signal and Oh model results vs soil moisture (mv), (d): difference between SAR signal
 410 and Oh model results vs incidence angle.

411 4.3. Evaluation of the IEM

412 The IEM was tested on our dataset using both a Gaussian correlation function (GCF) and an
 413 exponential correlation function (ECF). The evaluation of the IEM was carried out firstly using the
 414 entire dataset, later on for each radar wavelength (L-, C- and X-bands) and finally according to the
 415 validity domain of the IEM (Eq. 10).

416 Using all data, the IEM simulates the backscattering in HH polarization with an RMSE of 10.5
 417 dB and 5.6 dB for GCF and ECF, respectively (Table 4). At VV polarization, the RMSE is 9.2 dB for
 418 GCF and 6.5 dB for ECF. At HV polarization, the RMSE is higher than 30.0 dB for both GCF and
 419 ECF. Some points show a large discrepancy between the real data and the IEM simulations
 420 performed using both ECF and GCF (Figures 6-11). In case of the ECF (figures 9, 10, and 11), these
 421 points are mainly outside the IEM validity domain (Eq. 10). In case of GCF (Figures 6, 7, and 8), the
 422 huge error is due to the high sensitivity of the IEM to roughness parameters ($Hrms$ and L). Using
 423 the GCF, the IEM underestimates the backscattering coefficients for data with low $Hrms$ values
 424 ($kHrms < 3$), high L values ($L > 4$ cm) and with high incidence angle ($\theta > 35^\circ$). Using the ECF, the
 425 sensitivity of backscattering to the roughness parameters is much lower (Figures 9, 10 and 11).
 426 Altese *et al.* [67], Zribi *et al.* [23,68], and Callens *et al.* [69] showed that in agricultural areas, the ECF
 427 usually provides better agreement to real data than the GCF.

428 The results obtained in L-band show that the IEM simulates the backscattering in HH pol.
 429 using both GCF and ECF with differences between real data and model simulations ranges between
 430 -0.9 dB and +0.6 dB, with an RMSE of 3.6 dB for GCF and 2.9 dB for ECF (Table 4). At VV

431 polarization, the IEM overestimates the backscattering by about 2.5 dB and 1.3 dB for GCF and ECF,
432 respectively (RMSE of 5.0 dB for GCF and 3.5 dB for ECF). At HV polarization, the IEM simulates
433 the backscattering using GCF with RMSE of 14.5 dB using GCF, and lower RMSE (6.8 dB) using
434 ECF.

435 According to the results observed in C-band, the IEM simulates the backscattering using GCF
436 with RMSE of 11.2 dB and 8.6 dB for HH and VV polarizations, respectively (Table 4). The RMSE is
437 lower with ECF than GCF about 4.1 dB for HH and 4.9 dB for VV polarizations. At HV polarization,
438 the RMSE is higher than 25.0 dB using both GCF and ECF.

439 The results obtained in X-band show that the IEM simulates the backscattering with higher
440 RMSE than L- and C- bands, the RMSE in HH pol. being about 10.6 dB for GCF and 8.3 dB for ECF.
441 At VV polarization, the RMSE is 11.3 dB for GCF and 9.4 dB for ECF. At HV polarization, the IEM
442 simulates the backscattering with high RMSE which is larger than 54.0 dB using both GCF and ECF.

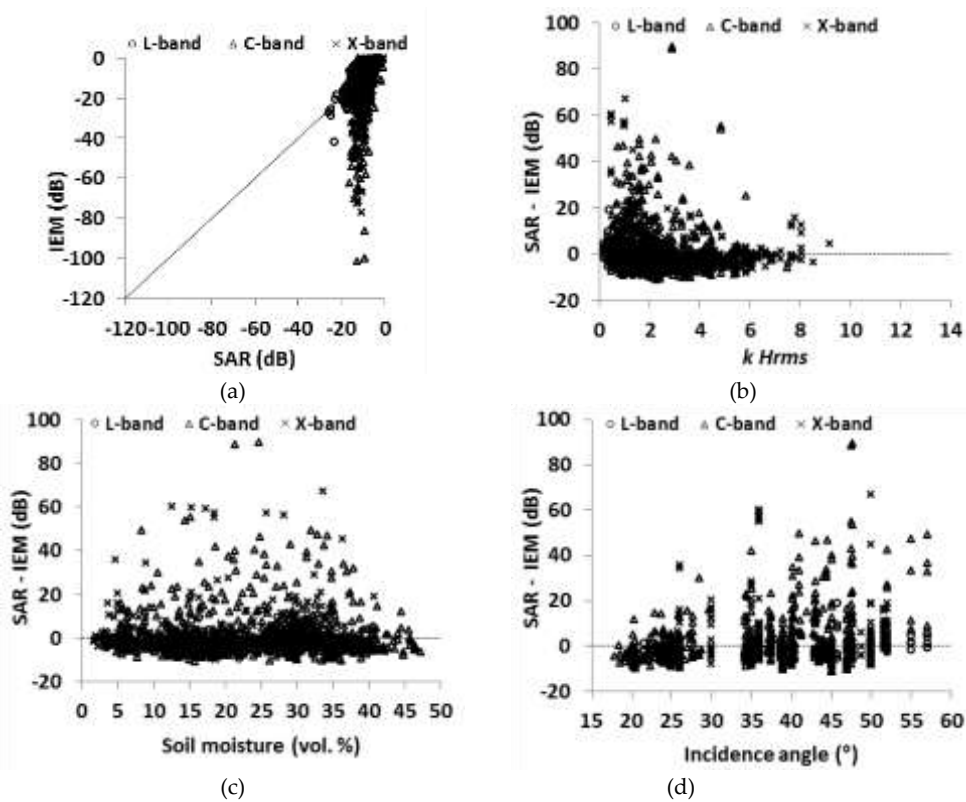
443 The analysis of the error was also studied according to the validity domain of the IEM (Eq. 10).
444 Inside the validity domain, the RMSE is larger than 11.5 dB for both HH and VV polarizations using
445 GCF. Better results were obtained using ECF, where the IEM correctly simulates the backscattering
446 at both HH and VV polarizations with differences between real and simulated data between -1.2 dB
447 and -0.9 dB with RMSE of 3.2 dB at HH and 3.7 dB at VV polarizations, using data concerning the
448 IEM validity domain. Outside the IEM validity domain, the IEM simulates the backscattering with
449 RMSE of 6.7 dB for HH and 3.1 dB for VV using GCF; whereas RMSE is 7.8 dB for HH and 9.4 dB for
450 VV polarization using ECF. At HV polarizations, model simulations show large differences from
451 real data for both GCF and ECF for points inside or outside the validity domain of the IEM (in this
452 case, RMSE is larger than 20 dB). Errors observed on IEM simulations were also studied as a
453 function of the difference between L_{opt} and the measured correlation length (L). Results show that
454 the IEM using GCF gives poor simulations mainly when the measured correlation length was over-
455 estimated ($L > L_{opt}$). In this case, the IEM strongly under-estimates the SAR backscatter. In addition,
456 the performance of the IEM was also analyzed using ECF according to the difference between L_{opt}
457 and L . Results show the same performance of the IEM whatever the difference between L_{opt} and
458 L . Error on IEM simulation was also studied as a function of the difference between L_{opt} and
459 $L_{measured}$. Results showed that the IEM gives poor simulations when L_{opt} is lower than
460 $L_{measured}$. Indeed, in the case of data with L_{opt} lower than $L_{measured}$, the IEM model strongly
461 over-estimates the SAR backscatter.

462 As a conclusion, we could say that the IEM better simulates the backscattering in L- band than
463 in C- and X-bands. Moreover, the results show a better fitting with real data using ECF instead than
464 GCF, which agrees with the validity domain of the IEM.
465

466
467
468

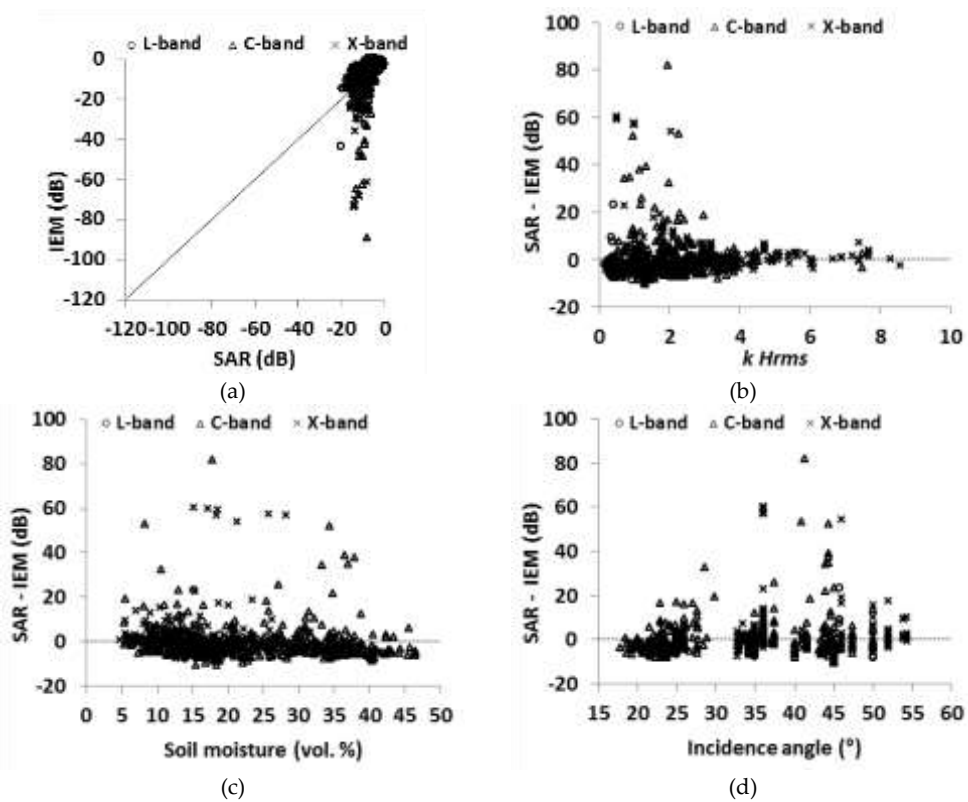
Table 4. Comparison between real data and IEM versions (original model, IEM_B and AIEM) using both GCF and ECF. (1) all data, (2) for different SAR wavelength, (3) according to the validity domain of IEM. Bias = real data – model simulations.

			<i>All data</i>	<i>L-band</i>	<i>C-band</i>	<i>X-band</i>	<i>inside the validity domain</i>	<i>outside the validity domain</i>
IEM using GCF	HH	Bias (dB)	+0.8	-0.9	+0.7	+1.5	+2.6	-1.8
		RMSE (dB)	10.5	3.6	11.2	10.6	12.4	6.7
	HV	Bias (dB)	+17.2	+5.2	+11.8	+46.3	+18.0	+14.1
		RMSE (dB)	38.4	14.5	26.7	74.0	28.5	50.1
	VV	Bias (dB)	+0.4	-2.5	+0.7	+3.5	+1.2	-0.9
		RMSE (dB)	9.2	5.0	8.6	11.3	11.5	3.1
IEM using ECF	HH	Bias (dB)	+0.8	+0.6	-1.0	+4.2	-1.2	+3.8
		RMSE (dB)	5.6	2.9	4.1	8.3	3.2	7.8
	HV	Bias (dB)	-15.8	+1.2	-19.9	0.0	-15.8	-17.1
		RMSE (dB)	31.4	6.8	25.1	54.4	20.1	44.3
	VV	Bias (dB)	+2.2	-1.3	+0.5	+6.7	-0.9	+7.1
		RMSE (dB)	6.5	3.5	4.9	9.4	3.7	9.4
IEM_B with Lopt using GCF	HH	Bias (dB)	-0.3	-0.1	-0.6	+0.3		
		RMSE (dB)	2.0	2.3	2.1	1.8		
	HV	Bias (dB)			-1.3			
		RMSE (dB)			3.1			
	VV	Bias (dB)	+0.1	+0.2	0	+0.3		
		RMSE (dB)	1.9	2.3	1.9	1.8		
AIEM using GCF	HH	Bias (dB)	+2.3	-3.2	+2.9	+3.1		
		RMSE (dB)	12.2	5.4	13.4	11.7		
	VV	Bias (dB)	0.0	-4.1	+0.5	+0.5		
		RMSE (dB)	10.8	5.9	11.4	11.0		
AIEM using ECF	HH	Bias (dB)	-2.3	-3.0	-3.6	+0.2		
		RMSE (dB)	4.4	4.4	4.6	4.2		
	VV	Bias (dB)	-1.8	-2.4	-2.3	-0.7		
		RMSE (dB)	3.8	4.4	3.8	3.7		



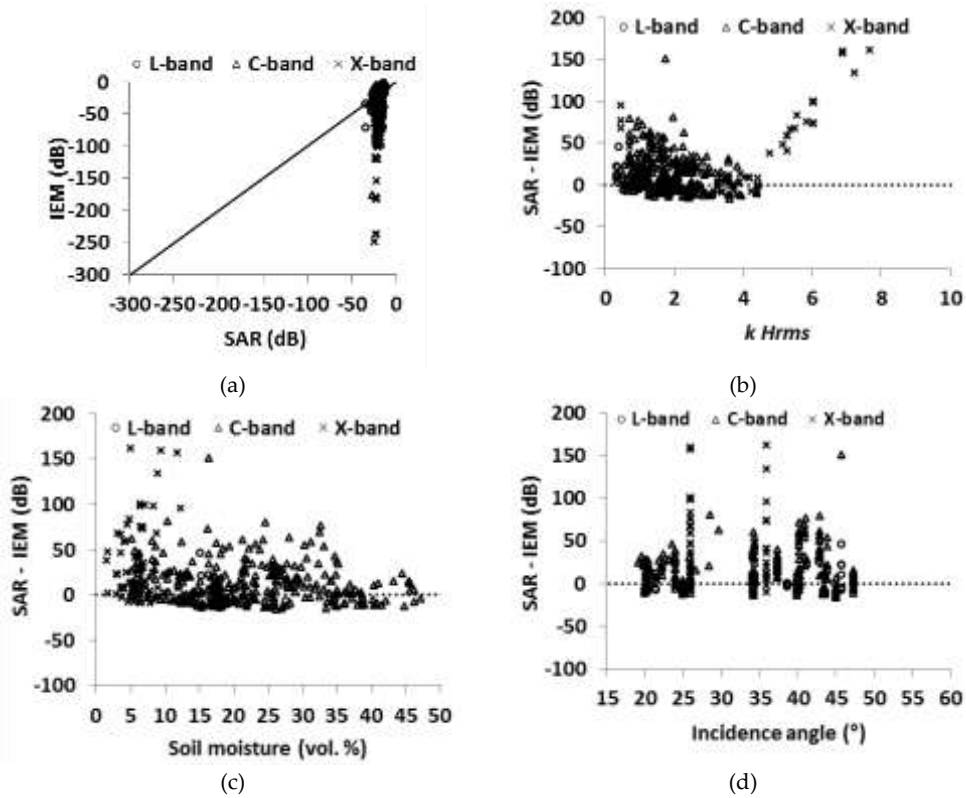
469 **Figure 6.** Comparison between backscattering coefficients derived from SAR images and those
 470 estimated from IEM at HH polarization using GCF. (a): IEM simulations vs SAR data, (b): difference
 471 between SAR signal and IEM vs soil roughness ($kHrms$), (c): difference between SAR signal and IEM
 472 vs soil moisture (mv), (d): difference between SAR signal and IEM vs incidence angle.

473

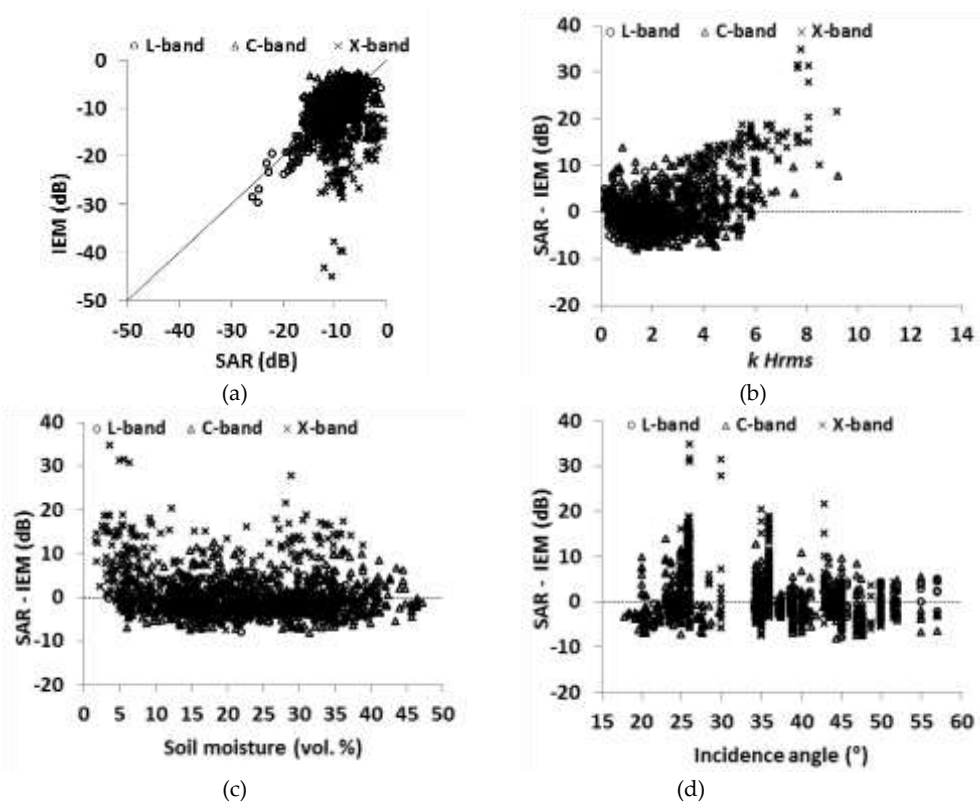


474 **Figure 7.** Comparison between backscattering coefficients derived from SAR images and those
 475 estimated from IEM at VV polarization using GCF. (a): IEM simulations vs SAR data, (b): difference
 476 between SAR signal and IEM vs soil roughness ($kHrms$), (c): difference between SAR signal and IEM
 477 vs soil moisture (mv), (d): difference between SAR signal and IEM vs incidence angle.

478

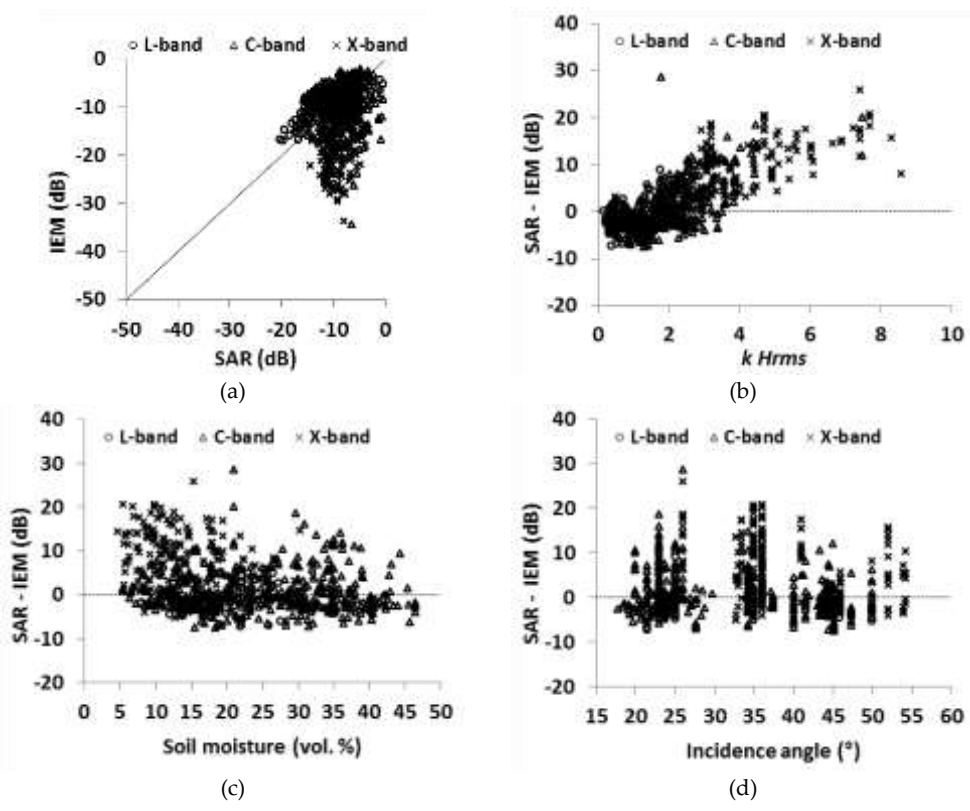


480 **Figure 8.** Comparison between backscattering coefficients derived from SAR images and those
 481 estimated from IEM at HV polarization using GCF. (a): IEM simulations vs SAR data, (b): difference
 482 between SAR signal and IEM vs soil roughness ($kHrms$), (c): difference between SAR signal and IEM
 483 vs soil moisture (mv), (d): difference between SAR signal and IEM vs incidence angle.



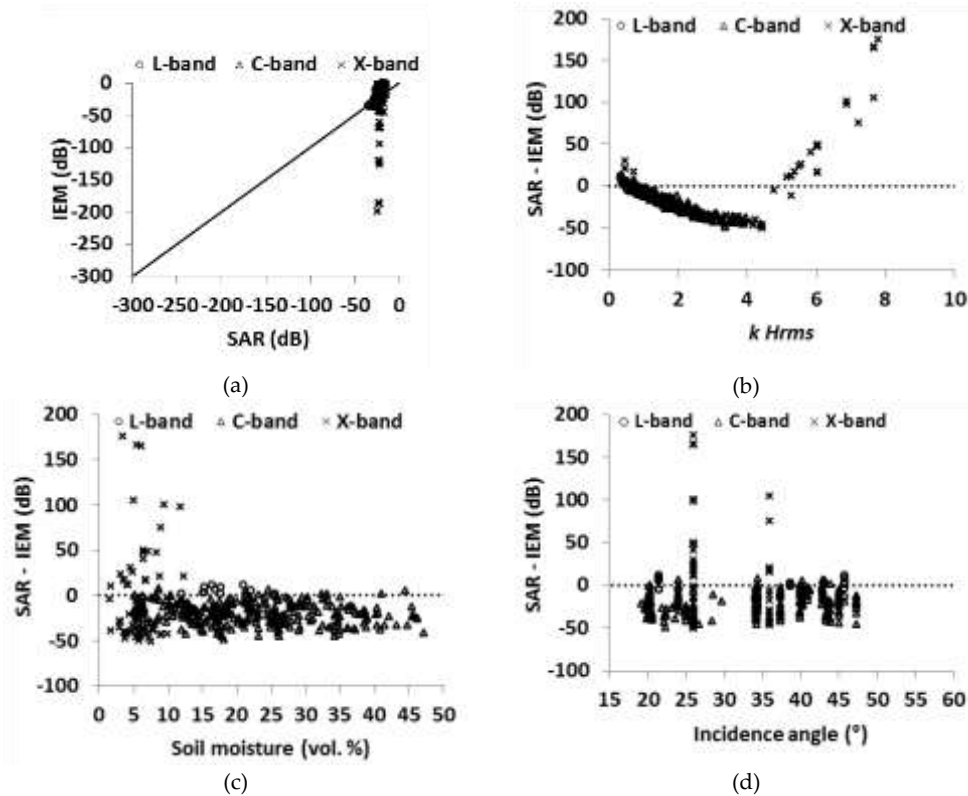
485 **Figure 9.** Comparison between backscattering coefficients derived from SAR images and those
 486 estimated from IEM at HH polarization using ECF. (a): IEM simulations vs SAR data, (b): difference
 487 between SAR signal and IEM vs soil roughness ($kHrms$), (c): difference between SAR signal and IEM
 488 vs soil moisture (mv), (d): difference between SAR signal and IEM vs incidence angle.

489



490 **Figure 10.** Comparison between backscattering coefficients derived from SAR images and those
 491 estimated from IEM at VV polarization using ECF. (a): IEM simulations vs SAR data, (b): difference
 492 between SAR signal and IEM vs soil roughness ($kHrms$), (c): difference between SAR signal and IEM
 493 vs soil moisture (mv), (d): difference between SAR signal and IEM vs incidence angle.

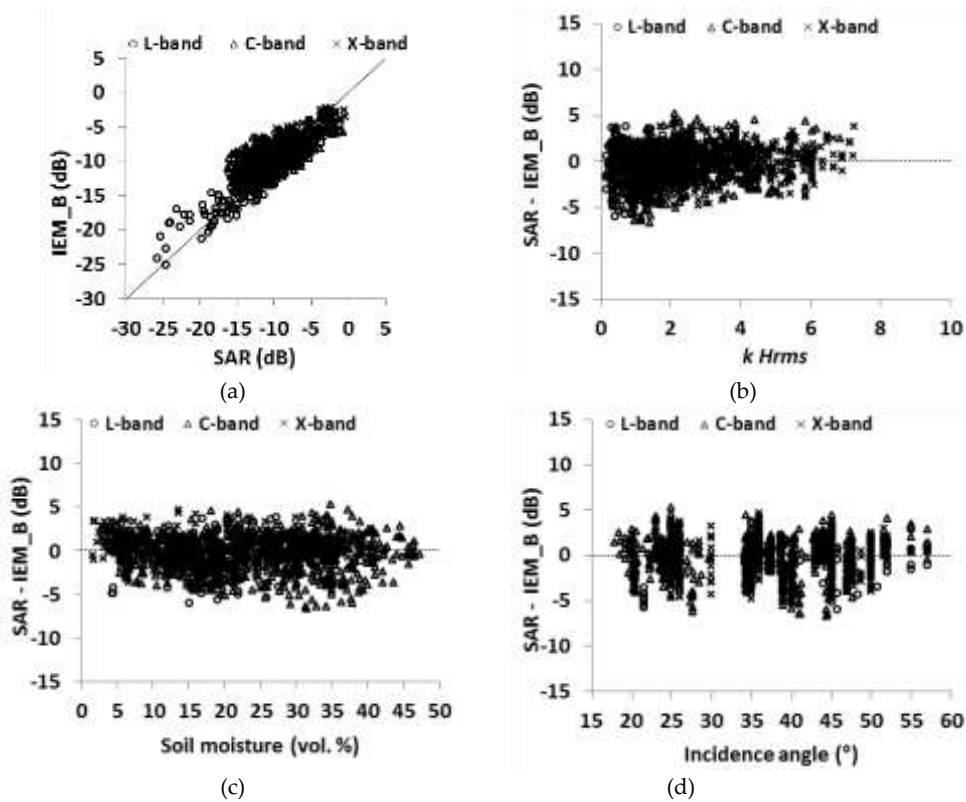
494



496 **Figure 11.** Comparison between backscattering coefficients derived from SAR images and those
 497 estimated from IEM at HV polarization using ECF. (a): IEM simulations vs SAR data, (b): difference
 498 between SAR signal and IEM vs soil roughness ($kHrms$), (c): difference between SAR signal and IEM
 499 vs soil moisture (mv), (d): difference between SAR signal and IEM vs incidence angle.

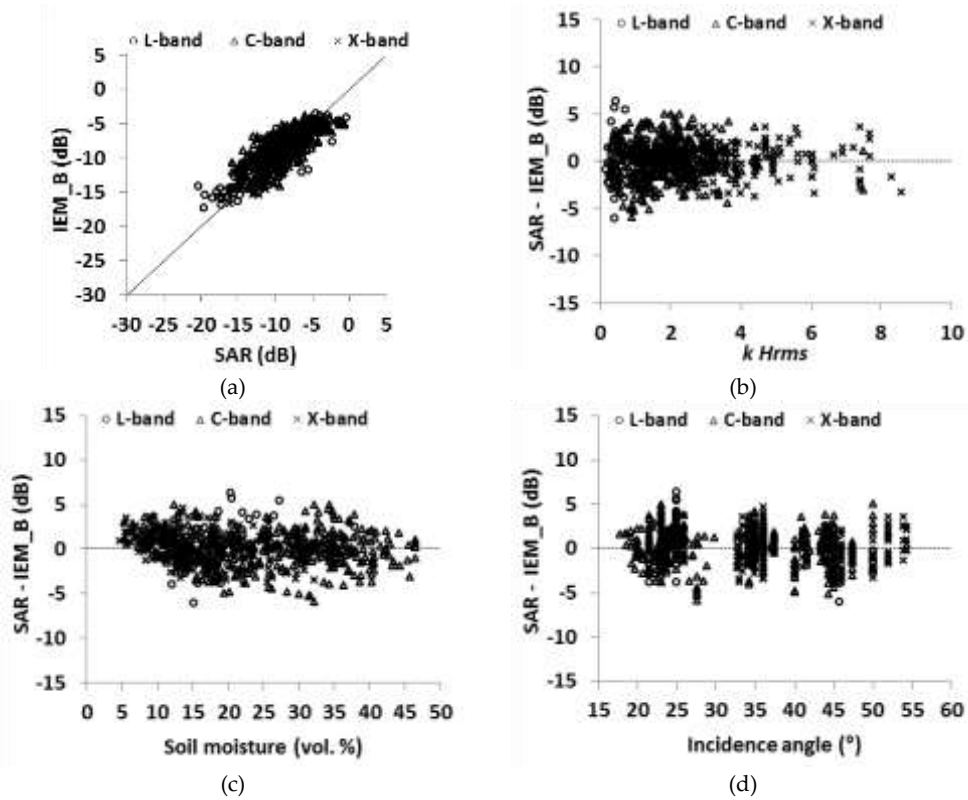
500 4.4. Evaluation of IEM modified by Baghdadi (IEM_B)

501 The IEM_B was also tested on our dataset. This model version was run using GCF (Figures 12,
 502 13 and 14). In comparison to the original IEM, results show that the RMSE was significantly lower.
 503 Using the entire dataset, the IEM_B correctly simulates the backscattering at both HH and VV
 504 polarizations showing low differences between real data and model simulations (-0.3 dB for HH
 505 and +0.1 dB for VV) with approximately similar RMSE of about 2.0 dB (Table 4). Moreover, the
 506 evaluation of the IEM_B was tested separately for each SAR band. Results show that the IEM_B
 507 correctly simulates the backscattering in comparison to the original model for all bands and in both
 508 HH and VV polarizations with a difference between real data and model simulations lower than 1.0
 509 dB and with approximately similar RMSE between 1.8 and 2.3 dB (Table 4). At HV polarization, the
 510 IEM_B slightly over-estimates the backscattering by about 1.3 dB with RMSE of 3.1 dB, (the IEM_B
 511 was run only at C-band). Moreover, results show that the IEM_B simulations in both HH and VV
 512 pol., are slightly better in X- and C-bands than in L-band. The analysis of the difference between
 513 IEM_B simulations and SAR data versus the difference between L_{opt} and the measured correlation
 514 length (L) shows that IEM_B simulates well SAR data whatever the value of the difference between
 515 L_{opt} and L . The analysis of the difference between IEM_B simulations and SAR data versus the
 516 difference between L_{opt} and the measured correlation length ($L_{measured}$) shows that IEM_B
 517 simulates well SAR data whatever the value of the difference between L_{opt} and $L_{measured}$.

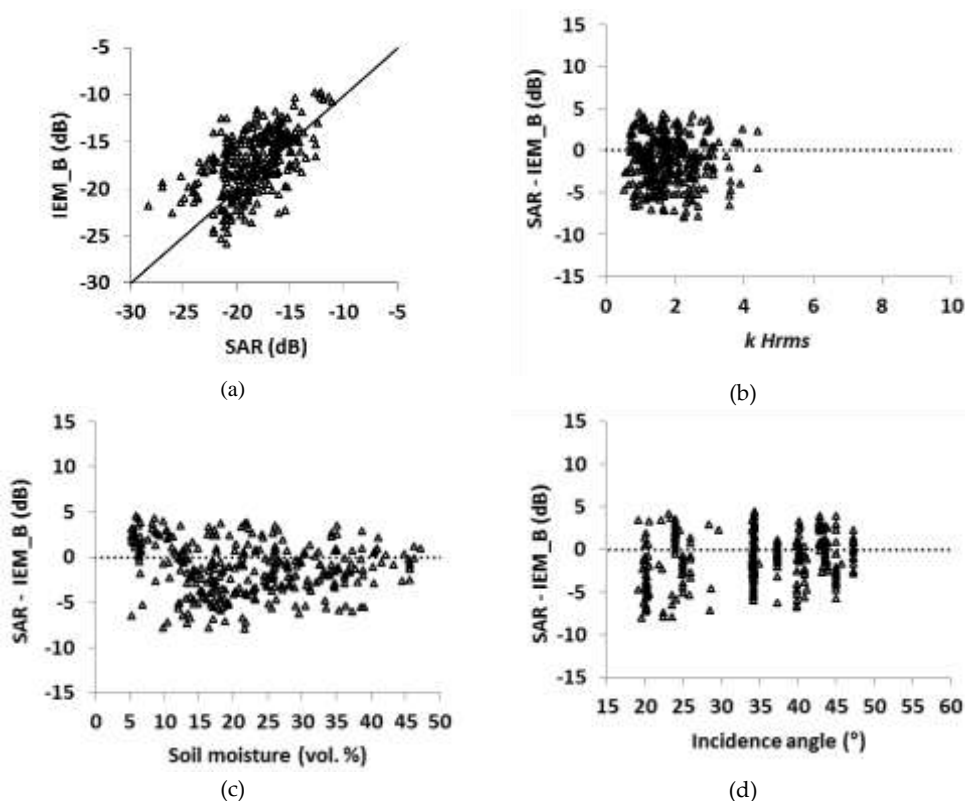


518 **Figure 12.** Comparison between backscattering coefficients derived from SAR images and those
 519 estimated from IEM_B at HH polarization using GCF. (a): IEM_B simulations vs SAR data, (b):
 520 difference between SAR signal and IEM_B vs soil roughness ($kHrms$), (c): difference between SAR
 521 signal and IEM_B vs soil moisture (mv), (d): difference between SAR signal and IEM_B vs incidence
 522 angle.

523



525 **Figure 13.** Comparison between backscattering coefficients derived from SAR images and those
 526 estimated from IEM_B at VV polarization using GCF. (a): IEM_B simulations vs SAR data, (b):
 527 difference between SAR signal and IEM_B vs soil roughness ($kHrms$), (c): difference between SAR
 528 signal and IEM_B vs soil moisture (mv), (d): difference between SAR signal and IEM_B vs incidence
 529 angle.



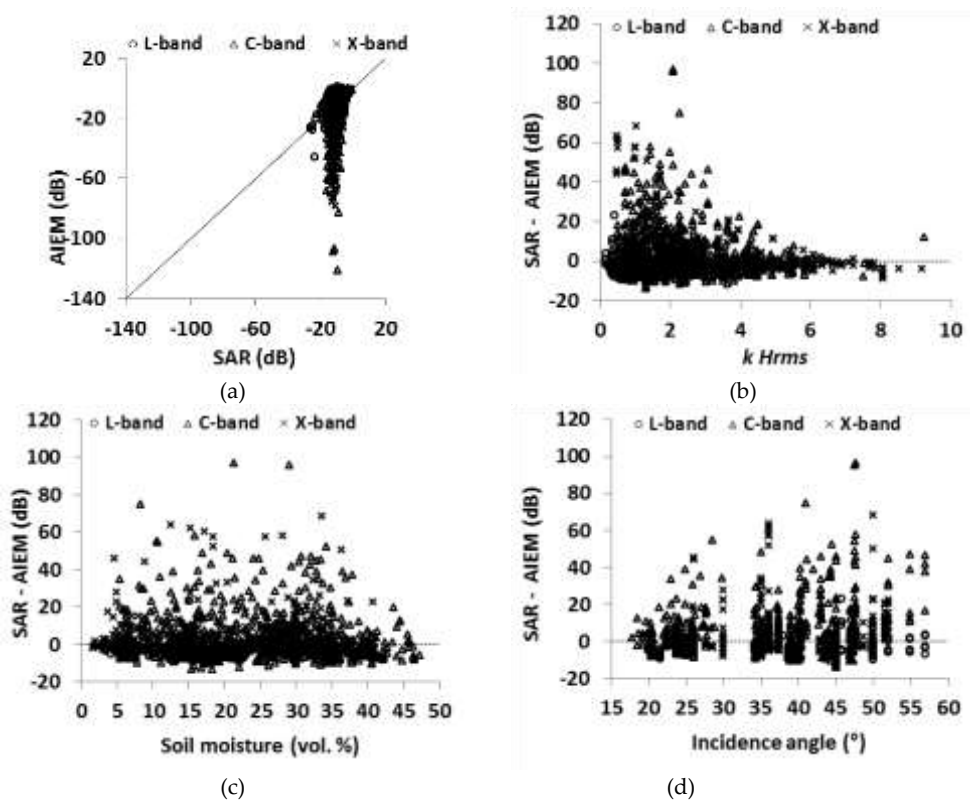
531 **Figure 14.** Comparison between backscattering coefficients derived from SAR images and those
 532 estimated from IEM_B in C-band at HV polarization using GCF. (a): IEM_B simulations vs SAR
 533 data, (b): difference between SAR signal and IEM_B vs soil roughness ($kHrms$), (c): difference
 534 between SAR signal and IEM_B vs soil moisture (mv), (d): difference between SAR signal and
 535 IEM_B vs incidence angle.

536 4.5. Evaluation of the Advanced Integral Equation Model (AIEM)

537 The AIEM was tested on our dataset at HH and VV polarizations using both GCF and ECF. For
 538 all data, the AIEM simulates the backscattering at HH and VV polarizations using GCF with RMSE
 539 larger than 10 dB (Table 4, Figures 15 and 16). Moreover, results show better agreements of the
 540 AIEM with real data using ECF (Figures 17 and 18). Indeed, the AIEM tends to overestimates the
 541 backscattering by about 2.3 dB at HH and 1.8 dB at VV (RMSE is 4.4 dB for HH and 3.8 dB for VV).
 542 Using the ECF, Figures 17 and 18 show high overestimations of the backscattering for low values of
 543 surface roughness ($kHrms < 4$) and for incidence angles higher than 35° . Moreover, Figures 17 et 18
 544 show high underestimation of the radar signal (using ECF) in both HH and VV polarizations for
 545 points with high surface roughness ($kHrms > 6$), low mv -values ($mv < 5$ vol.%, and with low incidence
 546 angles ($\theta < 20^\circ$). Figures 15 and 16 show that some points show high discrepancies between the real
 547 data and the AIEM simulations using GCF. Due to the high sensitivity to surface roughness of the
 548 AIEM using GCF, these points correspond mainly to surface with $kHrms < 3$, $L > 4$ cm and $\theta > 35^\circ$.

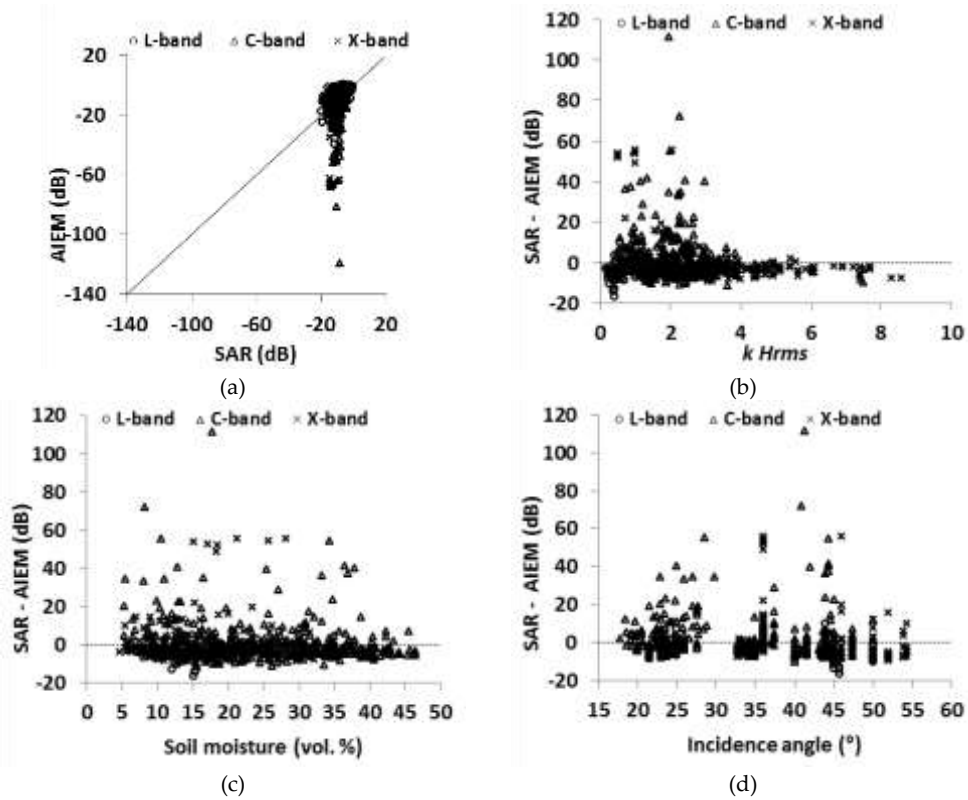
549 The performance of the AIEM was also evaluated for each SAR wavelength. Results show that
 550 in L-band the AIEM simulates the backscattering with RMSE of about 5.0 dB at both HH and VV
 551 polarizations using the GCF. In C and X-bands, the AIEM using GCF simulates the backscattering
 552 with RMSE higher than in L-band (RMSE > 11 dB). Moreover, AIEM better simulates better the
 553 backscattering in using GCF than ECF for all wavelength (RMSE about 4 dB).

554 In conclusions, the AIEM is able to better simulate better the backscattering than the original
 555 IEM only using the ECF with better results in X-band than in C- and L-bands.

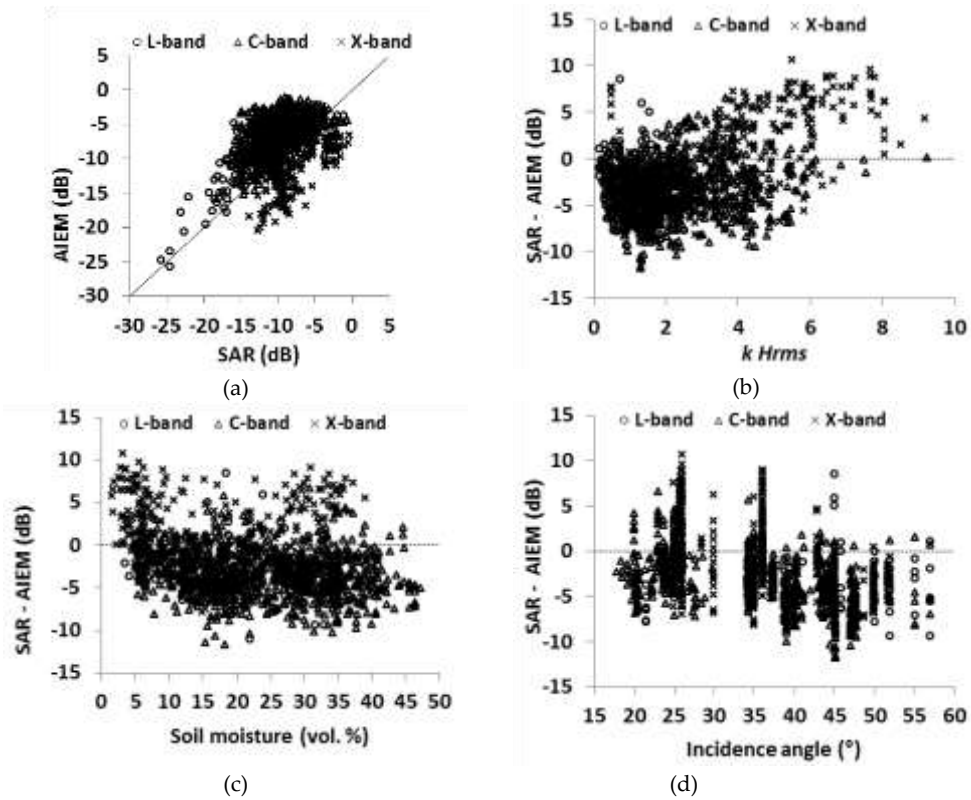


556 **Figure 15.** Comparison between backscattering coefficients derived from SAR images and those
 557 estimated from AIEM at HH polarization using GCF. (a): AIEM simulations vs SAR data, (b):
 558 difference between SAR signal and AIEM vs soil roughness ($kHrms$), (c): difference between SAR
 559 signal and AIEM vs soil moisture (mv), (d): difference between SAR signal and AIEM vs
 560 incidence angle.

561

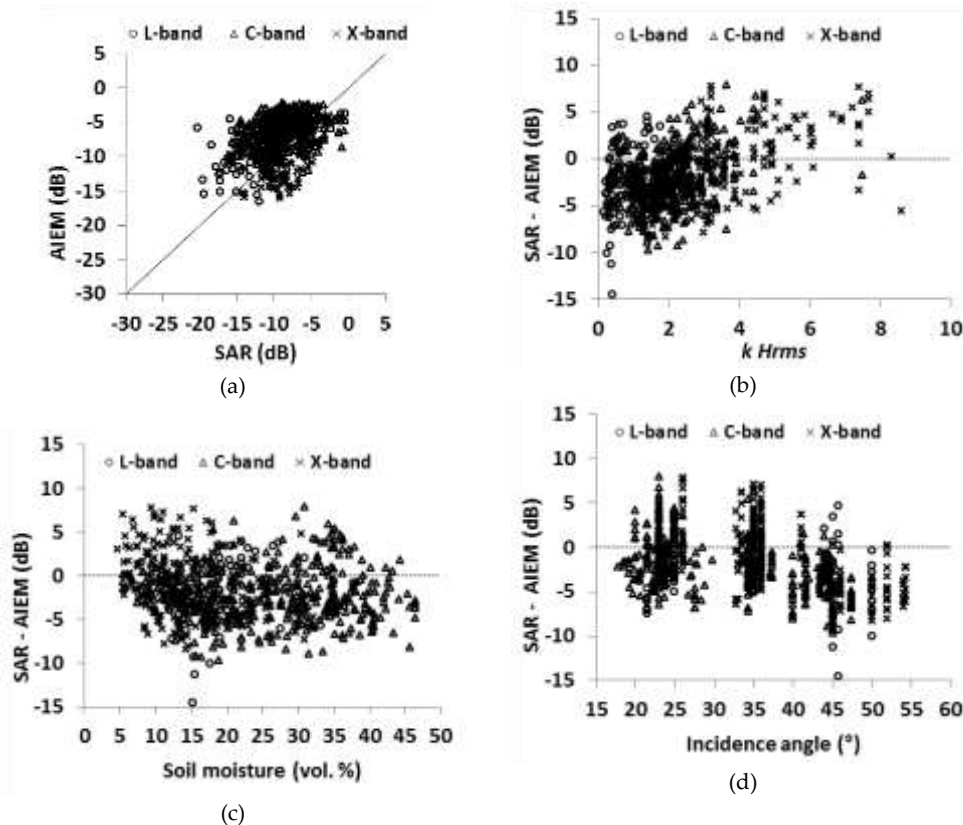


563 **Figure 16.** Comparison between backscattering coefficients derived from SAR images and those
 564 estimated from AIEM at VV polarization using GCF. (a): AIEM simulations vs SAR data, (b):
 565 difference between SAR signal and AIEM vs soil roughness ($kHrms$), (c): difference between SAR
 566 signal and AIEM vs soil moisture (mv), (d): difference between SAR signal and AIEM vs incidence
 567 angle.



570 **Figure 17.** Comparison between backscattering coefficients derived from SAR images and those
 571 estimated from AIEM at HH polarization using ECF. (a): AIEM simulations vs SAR data, (b):
 572 difference between SAR signal and AIEM vs soil roughness ($kHrms$), (c): difference between SAR
 573 signal and AIEM vs soil moisture (mv), (d): difference between SAR signal and AIEM vs incidence
 574 angle.

575



577 **Figure 18.** Comparison between radar backscattering coefficients calculated from SAR images and
 578 those estimated from AIEM for VV polarization using ECF. (a): AIEM simulations vs SAR data, (b):
 579 difference between SAR signal and AIEM vs soil roughness ($kHrms$), (c): difference between SAR
 580 signal and AIEM vs soil moisture (mv), (d): difference between SAR signal and AIEM vs incidence
 581 angle.

582 5. Conclusion

583 Physical (IEM, IEM_B and AIEM) and semi-empirical (Oh and Dubois) backscattering models
 584 were tested using a wide dataset composed by large intervals of surface conditions (mv between 2
 585 vol.% and 47 vol.%, $Hrms$ between 0.2 cm and 9.6 cm and $kHrms$ from 0.2 and 13.4), the dataset was
 586 acquired over bare soils in various agricultural study sites (France, Italy, Germany, Belgium,
 587 Luxembourg, Canada and Tunisia) characterized by large variety of climatological conditions and
 588 using SAR sensors in L-, C- and X-bands with incidence angle between 18 $^{\circ}$ and 57 $^{\circ}$.

589 Results show that the IEM modified by Baghdadi (IEM_B used the empirical correlation length
 590 instead of measured correlation length) provides the most accurate SAR simulations (bias lower
 591 than 1.0 dB and RMSE lower than 2.0 dB) with slightly better performance in X-band (RMSE=1.8
 592 dB) than in L- and C-bands (RMSE between 1.9 and 2.3 dB). At HV polarization, the IEM_B was
 593 only run at C-band. Results show that the RMSE strongly decreases from values higher than 25.1
 594 dB, using the original IEM, to 3.1 dB, using IEM_B. In contrast, high RMSE were found using both
 595 IEM and AIEM using Gaussian correlation function (RMSE higher than 9.2 dB) for both HH and VV
 596 polarizations because of the high sensitivity of the Gaussian correlation function to roughness
 597 parameters, mainly for $kHrms < 3$ and $L > 4$ cm. Moreover, results show better simulations of
 598 measured backscattering coefficients for both IEM and AIEM using exponential correlation function

599 (RMSE > 5.6 dB for IEM and RMSE > 3.8 dB for AIEM) at HH and VV polarizations. At HV
600 polarization, IEM results show very high errors (RMSE larger than 30.0 dB using both Gaussian
601 correlation function and exponential correlation function). The AIEM better simulates the
602 backscattering than the original IEM only using the exponential correlation function with slightly
603 better results in X-band than in C- and L-bands. In contrast, the IEM simulates better the
604 backscattering in L- band than C- and X-bands (Table 4).

605 Using the empirical models, all the Oh model versions show good agreements (RMSE<3.0 dB)
606 with measured backscattering with slightly better performance of the Oh 1992 version (bias less
607 than 1.0 dB and RMSE less than 2.6 dB) at both HH and VV polarizations. The Oh model provides
608 better results than Dubois model which simulates the backscattering in HH with RMSE of 4.0 dB,
609 and slightly better simulations for VV with RMSE of 2.9 dB. At HV polarization, the Oh 2002
610 version correctly simulates the backscattering with difference between real and simulated data of
611 about +0.7 dB and RMSE of 2.9 dB. The performance of the Oh 1992 version in HH and VV
612 polarizations is better in C- and X-bands (bias between -1.2 and +0.4 dB with RMSE <2.5 dB) than in
613 L-band (bias > +2.0 with RMSE >3.0 dB).

614 It should be mentioned that the use of different in situ sampling methods and SAR acquisition
615 techniques may also contribute to the modelling errors. Indeed, the datasets comprises both
616 airborne and space-borne acquisitions, which may cause scaling effects. In addition, in-situ data
617 have been collected using different techniques, both regarding soil moisture (gravimetric and TDR,
618 sometimes at different sampling depths) and roughness (different profile length and sampling
619 intervals, and post-processing methods).

620 This study evaluated the robustness of the most used backscattering models by means of
621 statistical indices (Bias and RMSE). These statistical indices should guide in choosing the
622 appropriate model for backscattering coefficients simulation. As it has been shown in the present
623 study, the IEM modified by Baghdadi (IEM_B) was the most accurate model among the others.
624 Thus, it is preferred to use the IEM_B in the inversion procedure of SAR backscattering coefficient
625 in order to more accurately estimate soil moisture and roughness parameters.
626

627 **Acknowledgment:** Authors are grateful to the space agencies for kindly providing the AIRSAR, SIR-C, JERS-1, ERS-
628 1/2, RADARSAT-1/2, ASAR, PALSAR-1, TerraSAR-X, COSMO-SkyMed, and ESAR data. This research is
629 supported by IRSTEA (National Research Institute of Science and Technology for Environment and
630 Agriculture), the French Space Study Center (CNES, TOSCA 2016), the French ANR (ANR AMETHYST
631 project) and the Belgian Science Policy Office (Contract SR/00/302). H. Lievens is a postdoctoral research of the
632 Research Foundation Flanders (FWO).

633 **Author Contributions:** Choker M. and Baghdadi N. conceived and designed the experiments; Choker M.
634 performed the experiments; Choker M. and Baghdadi N. analyzed the data; Zribi M., Paloscia S., Verhoest N.,
635 Lievens H., Mattia F. revised the manuscript; Choker M. wrote the paper.
636

637 References

- 638 1. Condrea, P.; Bostan, I. Environmental issues from an economic perspective. *Environ. Eng. Manag. J.* **2008**, *7*,
639 843–849.
- 640 2. Costantini, E. A. Soil indicators to assess the effectiveness of restoration strategies in dryland ecosystems.
641 *Solid Earth* **2016**, *7*, 397.
- 642 3. Lakshmi, V. Remote sensing of soil moisture. *ISRN Soil Sci.* **2013**, 2013.
- 643 4. Aubert, M.; Baghdadi, N.; Zribi, M.; Douaoui, A.; Loumagne, C.; Baup, F.; El Hajj, M.; Garrigues, S. Analysis
644 of TerraSAR-X data sensitivity to bare soil moisture, roughness, composition and soil crust. *Remote Sens.*
645 *Environ.* **2011**, *115*, 1801–1810.
- 646 5. Hajnsek, I.; Jagdhuber, T.; Schon, H.; Papathanassiou, K. P. Potential of estimating soil moisture under
647 vegetation cover by means of PolSAR. *IEEE Trans. Geosci. Remote Sens.* **2009**, *47*, 442–454.
- 648 6. Holah, N.; Baghdadi, N.; Zribi, M.; Bruand, A.; King, C. Potential of ASAR/ENVISAT for the characterization
649 of soil surface parameters over bare agricultural fields. *Remote Sens. Environ.* **2005**, *96*, 78–86.

- 650 7. Paloscia, S.; Pampaloni, P.; Pettinato, S.; Santi, E. A comparison of algorithms for retrieving soil moisture
651 from ENVISAT/ASAR images. *IEEE Trans. Geosci. Remote Sens.* **2008**, *46*, 3274–3284.
- 652 8. Oh, Y. Quantitative retrieval of soil moisture content and surface roughness from multipolarized radar
653 observations of bare soil surfaces. *IEEE Trans. Geosci. Remote Sens.* **2004**, *42*, 596–601.
- 654 9. Oh, Y.; Sarabandi, K.; Ulaby, F. T. An empirical model and an inversion technique for radar scattering from
655 bare soil surfaces. *IEEE Trans. Geosci. Remote Sens.* **1992**, *30*, 370–381.
- 656 10. Oh, Y.; Sarabandi, K.; Ulaby, F. T. An inversion algorithm for retrieving soil moisture and surface
657 roughness from polarimetric radar observation. In *Geoscience and Remote Sensing Symposium, 1994.*
658 *IGARSS'94. Surface and Atmospheric Remote Sensing: Technologies, Data Analysis and Interpretation., International;*
659 *IEEE, 1994; Vol. 3, pp. 1582–1584.*
- 660 11. Oh, Y.; Sarabandi, K.; Ulaby, F. T. Semi-empirical model of the ensemble-averaged differential Mueller
661 matrix for microwave backscattering from bare soil surfaces. *IEEE Trans. Geosci. Remote Sens.* **2002**, *40*, 1348–
662 1355.
- 663 12. Dubois, P. C.; Van Zyl, J.; Engman, T. Measuring soil moisture with imaging radars. *IEEE Trans. Geosci.*
664 *Remote Sens.* **1995**, *33*, 915–926.
- 665 13. Fung, A. K.; Li, Z.; Chen, K.-S. Backscattering from a randomly rough dielectric surface. *IEEE Trans. Geosci.*
666 *Remote Sens.* **1992**, *30*, 356–369.
- 667 14. Baghdadi, N.; King, C.; Chanzy, A.; Wigneron, J. P. An empirical calibration of the integral equation model
668 based on SAR data, soil moisture and surface roughness measurement over bare soils. *Int. J. Remote Sens.*
669 **2002**, *23*, 4325–4340.
- 670 15. Baghdadi, N.; Gherboudj, I.; Zribi, M.; Sahebi, M.; King, C.; Bonn, F. Semi-empirical calibration of the IEM
671 backscattering model using radar images and moisture and roughness field measurements. *Int. J. Remote*
672 *Sens.* **2004**, *25*, 3593–3623.
- 673 16. Baghdadi, N.; Holah, N.; Zribi, M. Calibration of the Integral Equation Model for SAR data in C-band and
674 HH and VV polarizations. *Int. J. Remote Sens.* **2006**, *27*, 805–816.
- 675 17. Baghdadi, N.; Chaaya, J. A.; Zribi, M. Semiempirical calibration of the integral equation model for SAR data
676 in C-band and cross polarization using radar images and field measurements. *IEEE Geosci. Remote Sens. Lett.*
677 **2011**, *8*, 14–18.
- 678 18. Baghdadi, N.; Saba, E.; Aubert, M.; Zribi, M.; Baup, F. Evaluation of radar backscattering models IEM, Oh,
679 and Dubois for SAR data in X-band over bare soils. *IEEE Geosci. Remote Sens. Lett.* **2011**, *8*, 1160–1164.
- 680 19. Baghdadi, N.; Zribi, M.; Paloscia, S.; Verhoest, N. E.; Lievens, H.; Baup, F.; Mattia, F. Semi-empirical
681 calibration of the integral equation model for co-polarized L-band backscattering. *Remote Sens.* **2015**, *7*,
682 13626–13640.
- 683 20. Chen, K.-S.; Wu, T.-D.; Tsang, L.; Li, Q.; Shi, J.; Fung, A. K. Emission of rough surfaces calculated by the
684 integral equation method with comparison to three-dimensional moment method simulations. *IEEE Trans.*
685 *Geosci. Remote Sens.* **2003**, *41*, 90–101.
- 686 21. Baghdadi, N.; Zribi, M. Evaluation of radar backscatter models IEM, OH and Dubois using experimental
687 observations. *Int. J. Remote Sens.* **2006**, *27*, 3831–3852.
- 688 22. Mattia, F.; Le Toan, T.; Souyris, J.-C.; De Carolis, C.; Floury, N.; Posa, F.; Pasquariello, N. G. The effect of
689 surface roughness on multifrequency polarimetric SAR data. *IEEE Trans. Geosci. Remote Sens.* **1997**, *35*, 954–
690 966.
- 691 23. Zribi, M.; Taconet, O.; Le Hégarat-Masclé, S.; Vidal-Madjar, D.; Emblanch, C.; Loumagne, C.; Normand, M.
692 Backscattering behavior and simulation comparison over bare soils using SIR-C/X-SAR and ERASME 1994
693 data over Orgeval. *Remote Sens. Environ.* **1997**, *59*, 256–266.
- 694 24. Mattia, F.; Davidson, M. W.; Le Toan, T.; D'Haese, C. M.; Verhoest, N. E.; Gatti, A. M.; Borgeaud, M. A
695 comparison between soil roughness statistics used in surface scattering models derived from mechanical and
696 laser profilers. *IEEE Trans. Geosci. Remote Sens.* **2003**, *41*, 1659–1671.
- 697 25. Verhoest, N. E.; Lievens, H.; Wagner, W.; Álvarez-Mozos, J.; Moran, M. S.; Mattia, F. On the soil roughness
698 parameterization problem in soil moisture retrieval of bare surfaces from synthetic aperture radar. *Sensors*
699 **2008**, *8*, 4213–4248.
- 700 26. Ulaby, F. T.; Dubois, P. C.; Van Zyl, J. Radar mapping of surface soil moisture. *J. Hydrol.* **1996**, *184*, 57–84.
- 701 27. Baghdadi, N.; Paillou, P.; Grandjean, G.; Dubois, P.; Davidson, M. Relationship between profile length and
702 roughness variables for natural surfaces. *Int. J. Remote Sens.* **2000**, *21*, 3375–3381.
- 703 28. Davidson, M. W.; Le Toan, T.; Mattia, F.; Satalino, G.; Manninen, T.; Borgeaud, M. On the characterization
704 of agricultural soil roughness for radar remote sensing studies. *IEEE Trans. Geosci. Remote Sens.* **2000**, *38*, 630–
705 640.
- 706 29. Le Toan, T.; Davidson, M.; Mattia, F.; Borderies, P.; Chenerie, I.; Manninen, T.; Borgeaud, M. Improved
707 observation and modelling of bare soil surfaces for soil moisture retrieval. *Earth Obs. Q.* **1999**, 20–24.

- 708 30. Lievens, H.; Verhoest, N. E. C.; Keyser, E. D.; Vernieuwe, H.; Matgen, P.; Alvarez-Mozos, J.; Baets, B. D.
709 Effective roughness modelling as a tool for soil moisture retrieval from C-and L-band SAR. *Hydrol. Earth*
710 *Syst. Sci.* **2011**, *15*, 151–162.
- 711 31. De Keyser, E.; Vernieuwe, H.; Lievens, H.; Alvarez-Mozos, J.; De Baets, B.; Verhoest, N. E. Assessment of
712 SAR-retrieved soil moisture uncertainty induced by uncertainty on modeled soil surface roughness. *Int. J.*
713 *Appl. Earth Obs. Geoinformation* **2012**, *18*, 176–182.
- 714 32. Verhoest, N. E. C.; De Baets, B.; Mattia, F.; Satalino, G.; Lucau, C.; Defourny, P. A possibilistic approach to
715 soil moisture retrieval from ERS synthetic aperture radar backscattering under soil roughness uncertainty.
716 *Water Resour. Res.* **2007**, *43*.
- 717 33. Lievens, H.; Verhoest, N. E. Spatial and temporal soil moisture estimation from RADARSAT-2 imagery
718 over Flevoland, The Netherlands. *J. Hydrol.* **2012**, *456*, 44–56.
- 719 34. Baghdadi, N.; Holah, N.; Zribi, M. Calibration of the Integral Equation Model for SAR data in C-band and
720 HH and VV polarizations. *Int. J. Remote Sens.* **2006**, *27*, 805–816.
- 721 35. Rahman, M. M.; Moran, M. S.; Thoma, D. P.; Bryant, R.; Sano, E. E.; Holifield Collins, C. D.; Skirvin, S.;
722 Kershner, C.; Orr, B. J. A derivation of roughness correlation length for parameterizing radar backscatter
723 models. *Int. J. Remote Sens.* **2007**, *28*, 3995–4012.
- 724 36. Panciera, R.; Tanase, M. A.; Lowell, K.; Walker, J. P. Evaluation of IEM, Dubois, and Oh radar backscatter
725 models using airborne L-band SAR. *IEEE Trans. Geosci. Remote Sens.* **2014**, *52*, 4966–4979.
- 726 37. Dong, L.; Baghdadi, N.; Ludwig, R. Validation of the AIEM through correlation length parameterization at
727 field scale using radar imagery in a semi-arid environment. *IEEE Geosci. Remote Sens. Lett.* **2013**, *10*, 461–465.
- 728 38. McNairn, H.; Merzouki, A.; Pacheco, A. Estimating surface soil moisture using Radarsat-2. *Int. Arch.*
729 *Photogramm. Remote Sens. Spat. Inf. Sci.* **2010**, *38*, 576–579.
- 730 39. Zribi, M.; Taconet, O.; Le Hégarat-Masclé, S.; Vidal-Madjar, D.; Emblanch, C.; Loumagne, C.; Normand, M.
731 Backscattering behavior and simulation comparison over bare soils using SIR-C/X-SAR and ERASME 1994
732 data over Orgeval. *Remote Sens. Environ.* **1997**, *59*, 256–266.
- 733 40. Baghdadi, N.; Dubois-Fernandez, P.; Dupuis, X.; Zribi, M. Sensitivity of main polarimetric parameters of
734 multifrequency polarimetric SAR data to soil moisture and surface roughness over bare agricultural soils.
735 *IEEE Geosci. Remote Sens. Lett.* **2013**, *10*, 731–735.
- 736 41. Baghdadi, N.; Zribi, M.; Loumagne, C.; Ansart, P.; Anguela, T. P. Analysis of TerraSAR-X data and their
737 sensitivity to soil surface parameters over bare agricultural fields. *Remote Sens. Environ.* **2008**, *112*, 4370–4379.
- 738 42. Baghdadi, N.; Aubert, M.; Zribi, M. Use of TerraSAR-X data to retrieve soil moisture over bare soil
739 agricultural fields. *IEEE Geosci. Remote Sens. Lett.* **2012**, *9*, 512–516.
- 740 43. Baghdadi, N.; Gherboudj, I.; Zribi, M.; Sahebi, M.; King, C.; Bonn, F. Semi-empirical calibration of the IEM
741 backscattering model using radar images and moisture and roughness field measurements. *Int. J. Remote*
742 *Sens.* **2004**, *25*, 3593–3623.
- 743 44. Baghdadi, N.; King, C.; Bourguignon, A.; Remond, A. Potential of ERS and RADARSAT data for surface
744 roughness monitoring over bare agricultural fields: application to catchments in Northern France. *Int. J.*
745 *Remote Sens.* **2002**, *23*, 3427–3442.
- 746 45. Le Morvan, A.; Zribi, M.; Baghdadi, N.; Chanzy, A. Soil moisture profile effect on radar signal
747 measurement. *Sensors* **2008**, *8*, 256–270.
- 748 46. Baghdadi, N.; Saba, E.; Aubert, M.; Zribi, M.; Baup, F. Comparison between backscattered TerraSAR signals
749 and simulations from the radar backscattering models IEM, Oh, and Dubois. *IEEE Geosci. Remote Sens. Lett.*
750 **2011**, *6*, 1160–1164.
- 751 47. Baghdadi, N.; Aubert, M.; Cerdan, O.; Franchistéguy, L.; Viel, C.; Eric, M.; Zribi, M.; Desprats, J. F.
752 Operational mapping of soil moisture using synthetic aperture radar data: application to the Touch basin
753 (France). *Sensors* **2007**, *7*, 2458–2483.
- 754 48. Zribi, M.; Gorrab, A.; Baghdadi, N.; Lili-Chabaane, Z.; Mougenot, B. Influence of radar frequency on the
755 relationship between bare surface soil moisture vertical profile and radar backscatter. *IEEE Geosci. Remote*
756 *Sens. Lett.* **2014**, *11*, 848–852.
- 757 49. Gorrab, A.; Zribi, M.; Baghdadi, N.; Mougenot, B.; Fanise, P.; Chabaane, Z. L. Retrieval of both soil moisture
758 and texture using TerraSAR-X images. *Remote Sens.* **2015**, *7*, 10098–10116.
- 759 50. Aubert, M.; Baghdadi, N. N.; Zribi, M.; Ose, K.; El Hajj, M.; Vaudour, E.; Gonzalez-Sosa, E. Toward an
760 operational bare soil moisture mapping using TerraSAR-X data acquired over agricultural areas. *IEEE J. Sel.*
761 *Top. Appl. Earth Obs. Remote Sens.* **2013**, *6*, 900–916.
- 762 51. Dong, L.; Baghdadi, N.; Ludwig, R. Validation of the AIEM through correlation length parameterization at
763 field scale using radar imagery in a semi-arid environment. *IEEE Geosci. Remote Sens. Lett.* **2013**, *10*, 461–465.

- 764 52. Mattia, F.; Le Toan, T.; Souyris, J.-C.; De Carolis, C.; Floury, N.; Posa, F.; Pasquariello, N. G. The effect of
765 surface roughness on multifrequency polarimetric SAR data. *IEEE Trans. Geosci. Remote Sens.* **1997**, *35*, 954–
766 966.
- 767 53. Baronti, S.; Del Frate, F.; Ferrazzoli, P.; Paloscia, S.; Pampaloni, P.; Schiavon, G. SAR polarimetric features of
768 agricultural areas. *Int. J. Remote Sens.* **1995**, *16*, 2639–2656.
- 769 54. Macelloni, G.; Paloscia, S.; Pampaloni, P.; Sigismondi, S.; De Matthaeis, P.; Ferrazzoli, P.; Schiavon, G.;
770 Solimini, D. The SIR-C/X-SAR experiment on Montespetoli: sensitivity to hydrological parameters. *Int. J.*
771 *Remote Sens.* **1999**, *20*, 2597–2612.
- 772 55. Paloscia, S.; Macelloni, G.; Pampaloni, P.; Sigismondi, S. The potential of C-and L-band SAR in estimating
773 vegetation biomass: the ERS-1 and JERS-1 experiments. *IEEE Trans. Geosci. Remote Sens.* **1999**, *37*, 2107–2110.
- 774 56. Oh, Y.; Kay, Y. C. Condition for precise measurement of soil surface roughness. *IEEE Trans. Geosci. Remote*
775 *Sens.* **1998**, *36*, 691–695.
- 776 57. Hallikainen, M. T.; Ulaby, F. T.; Dobson, M. C.; El-Rayes, M. A.; Wu, L.-K. Microwave dielectric behavior of
777 wet soil-part 1: empirical models and experimental observations. *IEEE Trans. Geosci. Remote Sens.* **1985**, 25–34.
- 778 58. Rakotoarivony, L.; Taconet, O.; Vidal-Madjar, D.; Bellemain, P.; Benallegue, M. Radar backscattering over
779 agricultural bare soils. *J. Electromagn. Waves Appl.* **1996**, *10*, 187–209.
- 780 59. Remond, A. Image SAR: potentialités d'extraction d'un paramètre physique du ruissellement, la rugosité
781 (modélisation et expérimentation). *Univ. Bourgogne Publ. BRGM* **1997**.
- 782 60. Rakotoarivony, L. Validation de modèles de diffusion électromagnétique: Comparaison entre simulations
783 et mesures radar hélicoptère sur des surfaces agricoles de sol nu, 1995.
- 784 61. Boisvert, J. B.; Gwyn, Q. H. J.; Chanzy, A.; Major, D. J.; Brisco, B.; Brown, R. J. Effect of surface soil moisture
785 gradients on modelling radar backscattering from bare fields. *Int. J. Remote Sens.* **1997**, *18*, 153–170.
- 786 62. Zribi, M.; Taconet, O.; Le Hégarat-Mascle, S.; Vidal-Madjar, D.; Emblanch, C.; Loumagne, C.; Normand, M.
787 Backscattering behavior and simulation comparison over bare soils using SIR-C/X-SAR and ERASME 1994
788 data over Orgeval. *Remote Sens. Environ.* **1997**, *59*, 256–266.
- 789 63. Baghdadi, N.; Chaaya, J. A.; Zribi, M. Semiempirical calibration of the integral equation model for SAR data
790 in C-band and cross polarization using radar images and field measurements. *IEEE Geosci. Remote Sens. Lett.*
791 **2011**, *8*, 14–18.
- 792 64. Baghdadi, N.; Zribi, M.; Paloscia, S.; Verhoest, N. E.; Lievens, H.; Baup, F.; Mattia, F. Semi-empirical
793 calibration of the integral equation model for co-polarized L-band backscattering. *Remote Sens.* **2015**, *7*,
794 13626–13640.
- 795 65. Fung, A. K. *Microwave Scattering and Emission Models and Their Applications*; Artech House, Incorporated,
796 1994.
- 797 66. Wu, T.-D.; Chen, K.-S.; Shi, J.; Fung, A. K. A transition model for the reflection coefficient in surface
798 scattering. *IEEE Trans. Geosci. Remote Sens.* **2001**, *39*, 2040–2050.
- 799 67. Altese, E.; Bolognani, O.; Mancini, M.; Troch, P. A. Retrieving soil moisture over bare soil from ERS 1
800 synthetic aperture radar data: Sensitivity analysis based on a theoretical surface scattering model and field
801 data. *Water Resour. Res.* **1996**, *32*, 653–661.
- 802 68. Zribi, M.; Baghdadi, N.; Holah, N.; Fafin, O. New methodology for soil surface moisture estimation and its
803 application to ENVISAT-ASAR multi-incidence data inversion. *Remote Sens. Environ.* **2005**, *96*, 485–496.
- 804 69. Callens, M.; Verhoest, N. E.; Davidson, M. W. Parameterization of tillage-induced single-scale soil
805 roughness from 4-m profiles. *IEEE Trans. Geosci. Remote Sens.* **2006**, *44*, 878–888.